

ResearchOnline@JCU

This file is part of the following reference:

Alabbasi, Alyaa (2015) *Enhanced degradation resistance of metallic magnesium using biocompatible coatings for implant applications*. MPhil thesis, James Cook University.

Access to this file is available from:

<http://researchonline.jcu.edu.au/41351/>

The author has certified to JCU that they have made a reasonable effort to gain permission and acknowledge the owner of any third party copyright material included in this document. If you believe that this is not the case, please contact

*ResearchOnline@jcu.edu.au and quote
<http://researchonline.jcu.edu.au/41351/>*

**ENHANCED DEGRADATION RESISTANCE OF METALLIC
MAGNESIUM USING BIOCOMPATIBLE COATINGS
FOR IMPLANT APPLICATIONS**

Thesis submitted

by

Alyaa Alabbasi

May 2015

For the degree of Masters of Philosophy

College of Sciences, Technology and Engineering

James Cook University, Australia

STATEMENT OF ACCESS

I, the undersigned, the author of this thesis, understand that James Cook University will make it available for use within the University Library and, by microfilm or via other means, allow access to users in other approved libraries. I understand that generally this thesis has protection under the copyright Act and wish to place no further restriction on access to this thesis.

May, 2015

Alyaa Alabbasi

STATEMENT ON SOURCES

Declaration

I declare that this thesis is my own work and has not been submitted in any form for another degree or diploma at any university or other institution of tertiary education. Information derived from the published or unpublished work of others has been acknowledged in the text and a list of references is given.

May, 2015

Alyaa Alabbasi

ELECTRONIC COPY

I, the undersigned, the author of this work, declare that the electronic copy of this thesis provided to the James Cook University Library is an accurate copy of the print thesis submitted, within limits of the technology available.

May, 2015

Alyaa Alabbasi

COPYRIGHT DECLARATION

I, the undersigned, the author of this work, declare that every reasonable effort has been made to gain permission and acknowledge the owners of copyright material. I would be pleased to hear from any copyright owner who has been omitted or incorrectly acknowledged.

May, 2015

Alyaa Alabbasi

ACKNOWLEDGEMENTS

I am extremely grateful to my supervisor, Associate Professor Bobby Mathan for his unwavering support, advice and guidance through this research. I would also like to acknowledge Professor Yinghe He for his support.

I would like to thank my fellow postgraduate students R. Walter, O. Kazum, A. Baloch and S. Liyanaarachchi for their support and friendship.

I sincerely thank my husband Maysam Alburqeba and my children Rania, Ayman and Fatima for their understanding, love and encouragement through the tough times. Finally, I would like to thank my brother Hussein Alabbasi and all my family members for their words of encouragement and prayers.

STATEMENT ON THE CONTRIBUTION OF OTHERS

Research supervisory team:

Associate Professor Bobby Mathan and Professor Yinghe He, College of Science,
Technology and Engineering, James Cook University.

Editorial support

Associate Professor Bobby Mathan

Mrs. Katharine Fowler

ABSTRACT

Magnesium is an attractive metallic material for temporary implant applications. Magnesium readily dissolves in the physiological environment, and the degradation product is a non-toxic substance which can be harmlessly excreted in the urine. In fact, magnesium is essential to human metabolism and is naturally found in bone tissues, and the mechanical properties of magnesium are close to those of natural bone. However, the degradation rate of pure magnesium is unacceptably high in physiological conditions (i.e., pH level (7.4–7.6) and high chloride concentration). Consequently, a magnesium implant will lose its mechanical integrity before the tissues have sufficiently healed.

In recent years, a significant amount of work has been carried out to improve the degradation resistance of magnesium through alloying. Even then the degradation resistance of magnesium alloys is not sufficiently high. In addition, researchers have shown that the localized degradation susceptibility of magnesium alloys could potentially affect the mechanical integrity of magnesium alloy implants during service. Consequently, there is a need for increasing the general and localized degradation resistance of magnesium-based implants during the initial stage of service.

In the current study, two types of biocompatible materials (polymer and ceramics) were used as coating materials on pure magnesium and/or its alloy to delay general and localized degradation during service. The degradation behavior of coated samples was evaluated using electrochemical methods in simulated body fluid (SBF). Firstly, polylactic acid (PLA) was coated on a biodegradable magnesium alloy, AZ91, using a spin coating technique. PLA coating enhanced the degradation resistance of the alloy. Increasing the PLA coating thickness was found to improve the degradation resistance,

but resulted in poor adhesion. Long-term EIS experiments of the PLA coated samples suggested that their degradation resistance gradually decreased with increase in SBF exposure time. In another attempt, plasma electrolytic oxidation (PEO) technique was used to coat silicate based material on pure magnesium. The PEO coating increased the polarization resistance (R_p) of magnesium by an order of magnitude under short-term exposure to SBF, and also reduced the corrosion current (i_{corr}) by 65%. However, the coating failed to perform under long-term exposure due to the porous structure of the coating. To enhance the performance of the PEO coating, biocompatible materials such as polymer/calcium phosphate were coated on top of the porous PEO layer. *In vitro* degradation test results showed that the dual layer coatings were very effective in reducing both the localized and general degradation of the base metal even under long-term exposure.

The findings from this dissertation have been disseminated through the following publications.

Journal Papers:

- A. Alabbasi, S. Liyanaarachchi, M. Bobby Kannan “Polylactic acid coating on a biodegradable magnesium alloy: An *in vitro* degradation study by electrochemical impedance spectroscopy” *Thin Solid Films* 520 (2012) 6841-6844.
- A. Alabbasi, M. Bobby Kannan, R. Walter, M. Störmer, C. Blawert. “Performance of pulsed constant current silicate-based PEO coating on pure magnesium in simulated body fluid” *Materials Letters* 106 (2013) 18-21.

- A. Alabbasi, M. Bobby Kannan, A. Mehjabeen, C. Blawert “Biodegradable polymer sealing of porous PEO coating on pure magnesium: An *in vitro* degradation study” Applied Surface Science 180 (2013) 54-58.
- A. Alabbasi, M. Bobby Kannan, C. Blawert “Dual layer inorganic coating on magnesium for delaying the biodegradation for bone fixation implants” Materials Letters 124(2014)188–191.

TABLE OF CONTENTS

Statement of Access	iii
Statement on Sources	iv
Electronic Copy	v
Copyright Declaration	vi
Statement on the Contribution of Others.....	viii
Abstract.....	ix
Table of Contents	xii
List of Figures.....	xv
List of Tables.....	xvii
List of Symbols.....	xviii
CHAPTER 1: Introduction.....	1
1.1 Background.....	1
1.2 Objectives	3
CHAPTER 2 Literature Review	4
2.1 Magnesium	4
2.1.1 Degradation	5
2.1.2 Degradation Control.....	6
2.1.2.1 Alloying.....	6
2.1.2.2 Coatings.....	7
2.2 Biodegradable Polymers.....	8
2.2.1 Polylactic Acid (PLA).....	8
2.2.1.1 Degradation	9
2.2.1.2 PLA on Magnesium.....	10
2.3 Plasma Electrolytic Oxidation.....	10
2.3.1 PEO Coating Structure.....	11

2.3.2	PEO on Magnesium	12
2.4	Calcium Phosphate	14
2.4.1	CaP on Magnesium	14
2.5	Electrochemical Corrosion Techniques.....	18
2.5.1	Potentiodynamic Polarisation Method	18
2.5.2	Electrochemical Impedance Spectroscopy (EIS)	19
CHAPTER 3	Materials and Experimental Procedure	22
3.1	Materials	22
3.2	Coatings.....	22
3.2.1	Polymer Coating	22
3.2.2	Plasma Electrolytic Oxidation (PEO) Coating.....	23
3.2.3	Calcium Phosphate (CaP) Coating.....	23
3.2.4	Coating Characterization.....	23
3.3	In-vitro Degradation	23
CHAPTER 4	Single Layer Coatings	26
4.1	Polymer Coating.....	26
4.1.1	EIS Degradation.....	26
4.1.2	EIS Long-term Degradation.....	29
4.2	PEO Coating.....	31
4.2.1	Coating Morphology	31
4.2.2	EIS Degradation.....	32
4.2.3	Potentiodynamic Polarisation	34
4.2.4	Post-degradation Analysis.....	35
4.2.5	EIS Long-term Degradation.....	38
4.3	Summary.....	38
CHAPTER 5	Dual Layer Coatings.....	40
5.1	Polymer Coating on PEO	40

5.1.1	EIS In-vitro Degradation.....	40
5.1.2	Potentiodynamic Polarisation	43
5.1.3	EIS Long-term Degradation.....	44
5.1.4	Post-degradation Analysis.....	46
5.1.5	Degradation Mechanism	47
5.2	Calcium Phosphate (CaP) Coating on PEO.....	49
5.2.1	Morphology.....	49
5.2.2	Coating Characterization.....	51
5.2.3	EIS In-vitro Degradation.....	51
5.2.4	Potentiodynamic Polarisation	52
5.2.5	EIS Long-term Degradation.....	54
5.2.6	Post-degradation Analysis.....	55
5.3	Summary.....	58
CHAPTER 6 Conclusions		59
References		60

LIST OF FIGURES

Figure 2.1 Nyquist plots of magnesium and its alloys in simulated body fluid (Walter and Kannan, 2011).....	7
Figure 2.2 Bulk degradation of polylactic acid.	10
Figure 2.3 Nyquist plots of bare metal and the calcium phosphate coated magnesium alloy tested in SBF at 37 °C (Kannan and Wallipa, 2013).	16
Figure 2.4 A typical potentiodynamic polarisation scan	19
Figure 2.5 A typical Nyquist plot	20
Figure 3.1 Schematic representation of the three-step spin coating method.	22
Figure 3.2 (a) Schematic and (b) photograph of the three-electrode cell used for <i>in vitro</i> degradation experiments.....	25
Figure 4.1 Nyquist plots of: (a) AZ91 magnesium alloy, and (b) PLA coated magnesium alloy samples, after a 2 h immersion in SBF.	27
Figure 4.2 Equivalent circuits used for modelling EIS spectra of (a) AZ91 magnesium alloy and (b) PLA coated magnesium alloy samples, obtained after a 2 h immersion in SBF.	28
Figure 4.3 Polarisation resistance (R_p) of PLA coated (different thickness) alloy samples after a 2 h immersion in SBF.....	29
Figure 4.4 Polarisation resistance (R_p) of AZ91 magnesium alloy and PLA coated magnesium alloy samples, after different immersion intervals in SBF.....	31
Figure 4.5 SEM Micrographs of PEO coating on pure magnesium: (a) low magnification and (b) high magnification.	32
Figure 4.6 Nyquist plots of pure magnesium and PEO coated magnesium exposed to SBF.	33
Figure 4.7 Potentiodynamic polarisation plots for the pure magnesium and PEO coated magnesium exposed to SBF.	35
Figure 4.8 Post-degradation SEM micrographs of: (a,b) pure magnesium and (c,d) PEO coated magnesium	37
Figure 4.9 XRD spectra of PEO coated magnesium before and after exposure to SBF.	37
Figure 4.10 Polarisation resistance (R_p) of pure magnesium and PEO coated samples after different immersion intervals.	38

Figure 5.1 Nyquist plots of (a) pure Mg and PEO coated sample, and (b) PEO-PLLA coated sample, after 2 h immersion in SBF.....	41
Figure 5.2 Potentiodynamic polarisation curves of pure magnesium, PEO coated and PEO-PLLA coated samples after 2 h immersion in SBF.	44
Figure 5.3 Polarisation resistances (R_p) of pure magnesium, PEO coated and PEO-PLLA coated samples after different immersion intervals in SBF.....	46
Figure 5.4 Photographs of pure magnesium and PEO coated sample after 48 h exposure in SBF, and PEO-PLLA coated sample after 100 h exposure in SBF	47
Figure 5.5 Schematic representations of the <i>in vitro</i> degradation processes of pure magnesium, PEO coated and PEO-PLLA coated samples.....	48
Figure 5.6 SEM micrographs of the coatings on pure magnesium: (a and b) PEO coating, and (c and d) PEO-CaP coating.	50
Figure 5.7 FTIR spectra of PEO and PEO-CaP coatings on pure magnesium.....	51
Figure 5.8 Nyquist plots of pure magnesium, PEO coated and PEO-CaP coated magnesium samples exposed to SBF	53
Figure 5.9 Potentiodynamic polarisation plots of pure magnesium, PEO coated and PEO-CaP coated magnesium samples exposed to SBF.	53
Figure 5.10 Polarisation resistance (R_p) of pure magnesium, PEO coated and PEO-CaP coated magnesium samples after different immersion intervals in SBF.	55
Figure 5.11 Post-degradation SEM micrographs of coated pure magnesium: (a and b) PEO coated, and (c and d) PEO-CaP coated.	57

LIST OF TABLES

Table 2.1 Physical and mechanical properties of different implants materials in comparison with natural bone (Staiger et al., 2006).....	4
Table 2.2 Summary of PEO coatings on magnesium alloys.....	13
Table 3.1 Chemical composition of the simulated body fluid.....	24
Table 4.1 EIS fitting results for pure magnesium and PEO coated samples exposed to SBF.....	34
Table 5.1 EIS fitting results for the pure magnesium, PEO coated and PEO-PLLA coated samples exposed for 2h in SBF.....	42
Table 5.2 Electrochemical data for pure magnesium, PEO coated and PEO-PLLA coated samples from potentiodynamic polarization curves.....	44
Table 5.3 Electrochemical data for pure magnesium, PEO coated and PEO-CaP coated samples from potentiodynamic polarization curves.....	54

LIST OF SYMBOLS

$^{\circ}\text{C}$	=	Degree Celsius
Wt. %	=	Weight in percentage
PEO	=	Plasma electrolytic oxidation
PLLA	=	Poly (L-lactic acid)
CaP	=	Calcium Phosphate
EIS	=	Electrochemical impedance spectroscopy
E_0, E_t	=	Potential of the signal at given time
I_0, I_t	=	Current at given time
Z_0, Z_t	=	Impedance of the signal at given time
Φ	=	Phase shift between current and potential
CR	=	Corrosion rate
P	=	Density of the metal in g/cm^3
XRD	=	X-ray diffraction
SiC	=	Silicon-carbide
SEM	=	Scanning electron microscope
R_{pm}	=	Revolutions per minute
<i>FTIR</i>	=	Fourier transform infrared spectroscopy
OCP	=	Open circuit potential
R_s, R_f, R_{cb}, R_p	=	Resistance due to solution, film, charge transfer and polarisation
C_f, C_{dl}	=	Film capacitance, double layer capacitance
E_{corr}	=	Corrosion potential
i_{corr}	=	Corrosion current density
<i>Min</i>	=	Minute
<i>H</i>	=	Hour
<i>SBF</i>	=	Simulated body fluid

CHAPTER 1:INTRODUCTION

1.1 Background

Metallic materials have played an essential role in the orthopedic and biomedical field for many decades. The major types of metallic materials encompassing a wide range of applications as orthopedic implants are stainless steel, titanium alloys and cobalt-chromium alloys (Staiger et al., 2006). These metallic implants, categorized as permanent or non-degradable implants, have been used for extended service in, for example, hip implants and long-bone replacements. However, after the healing of the bone is complete, non-degradable implants such as screws, pins and plates may require a second surgical procedure for removal of the implant to avoid any complications due to metal dissolution/wear (Witte et al., 2008). The second surgical procedure will not only increase the risk of patient morbidity, but the holes in the bone due to implant removal could lead to re-fracture of the bone. The need to avoid this second surgical procedure has focused interest on research into biodegradable materials for temporary implant applications (Witte et al., 2005; Song G, 2007; Kannan and Raman, 2008a; Walter and Kannan, 2011; Nair and Laurencin, 2007; Gupta et al., 2007)

Biodegradable polymers such as polylactide (PLA) and polyglycolide (PGA) have been extensively researched for medical applications (Nair and Laurencin, 2007). These polymers are biocompatible in that they undergo hydrolytic degradation in body fluids, and the by-products of this degradation are nontoxic (Gupta et al., 2007; Zhang et al., 1994). However, these polymers possess poor mechanical properties as compared to those of natural bone (Witte et al., 2008), a major drawback in utilizing them as implants for load-bearing orthopedic applications.

Magnesium is a metallic material with physical and mechanical properties similar to natural bone (Witte et al., 2008; Saris et al., 2000). With attractive properties such as biodegradability and biocompatibility, researchers have been eager to investigate magnesium-based materials for potential biodegradable implant applications. Unfortunately, the high degradation rate of magnesium in physiological conditions (i.e., pH level (7.4–7.6) and high chloride concentration) is a major concern (Witte et al., 2008). Therefore current research has largely focused on controlling the degradation rate of magnesium by traditional methods such as alloying (Witte et al., 2005; Kannan and Raman, 2008a; Walter and Kannan, 2011) and the provision of coatings (Kannan, 2012b; Alabbasi et al., 2012; Hornberger et al., 2012).

In recent years, a number of magnesium alloys (containing elements such as Al, Ca, Zn, Mn and rare-earths) have been tested under *in vitro* and *in vivo* conditions. Alloying has decreased the general degradation rate of magnesium to some extent, but it remains prone to localized degradation (Kannan, 2010). Localized degradation is highly undesirable since it can potentially affect the mechanical integrity of the implant. Hence, a biodegradable coating on magnesium and magnesium-based materials is essential for reducing the localized degradation susceptibility during the initial service period of the implant.

1.2 Objectives

The main research objectives of this study were to:

- Coat biodegradable polymeric and/or ceramic materials on magnesium and/or its alloy using different coating methods.
- Evaluate the *in vitro* degradation behavior of the coated samples using electrochemical techniques in simulated body fluid.

CHAPTER 2 LITERATURE REVIEW

2.1 Magnesium

Magnesium is an attractive material for biodegradable implant applications due to its biocompatibility and biodegradability (Witte et al., 2008; Saris et al., 2000). As shown in Table 2.1, magnesium is a relatively low-density metal which has remarkably similar properties to natural bone. Also, magnesium has a closer elastic modulus to natural bone than the other metallic biomaterials, which may reduce its stress-shielding effects. Importantly, magnesium readily dissolves in the physiological environment, and the degradation product is a non-toxic substance, which is harmlessly excreted in the urine (Saris et al., 2000). In fact, magnesium is necessary for a variety of physiological functions, and also essential to human metabolism (Wolf and Cittadini, 2003).

Table 2.1 Physical and mechanical properties of different implant materials in comparison with natural bone (Staiger et al., 2006).

Material	Density (g/cm ³)	Elastic modulus (GPa)	Compressive yield strength(Mpa)	Fracture toughness (MPa.m ^{1/2})
Natural bone	1.8-2.1	3-20	130-180	3-6
Magnesium	1.74-2.0	41-45	65-100	15-40
Ti alloys	4.4-4.5	110-117	758-1117	55-115
Co-Cr alloys	8.3-9.2	230	450-1000	N/A
Stainless steel	7.9-8.1	189-205	170-310	50-200
Hydroxyapatite	3.1	73-117	600	0.7

2.1.1 Degradation

The degradation rate of pure magnesium is unacceptably high in physiological conditions (i.e., pH level (7.4–7.6) and high chloride concentration) (Witte et al., 2008; Kannan, 2010). Kannan (2010) also reported that the degradation rate of pure magnesium in SBF is 22mm/year. Although biodegradable biomaterials are required to dissolve with time, they need to degrade slowly so that their mechanical integrity is not affected during service. The degradation reactions of magnesium in an aqueous environment are given below (Zeng et al., 2008):

Anodic reaction (oxidation)



Cathodic reaction (reduction)

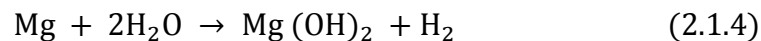


Product formation:

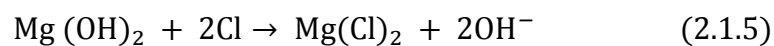


Magnesium dissolves in aqueous solutions by an electrochemical reaction with water, producing magnesium hydroxide and hydrogen gas. This reaction is relatively insensitive to oxygen concentration.

Overall reaction:



Magnesium hydroxide film forms a relatively protective layer on magnesium, but in the presence of chloride ions (30mmol/L), magnesium hydroxide will convert into highly soluble magnesium chloride (Witte et al., 2008).



It should be noted that the chloride concentration in body fluid is about 150 mmol/L. As a result, magnesium will suffer from severe corrosion (Witte et al., 2008). The rapid corrosion of magnesium will also produce hydrogen bubbles; hydrogen evolution reaction is the predominant cathodic reaction. This reaction will increase the local pH and potentially lead to local inflammation to the host tissues.

2.1.2 Degradation Control

A significant amount of work has been carried out over the past decade to reduce the degradation rate of magnesium by traditional methods such as alloying or coating the magnesium (Witte et al., 2005; Kannan and Raman, 2008a; Walter and Kannan, 2011).

2.1.2.1 Alloying

Magnesium's mechanical properties and degradation resistance can be modified by the addition of alloying elements. Magnesium compounds containing alloying elements such as Al, Zn, Mn, Ca and rare-earth elements have been widely studied (Kannan and Raman, 2008a; Witte et al., 2005; Walter and Kannan, 2011). The AZ series (containing aluminum-zinc) Mg alloys are popular due to their commercial availability. Alloying with aluminum produces beneficial role in the corrosion behavior of magnesium, and it also provides both solid solution strengthening and precipitation hardening (Witte et al., 2008). Zinc also increases the strength of the alloy (Witte et al., 2008). Out of all the AZ series alloys, the AZ91 alloy is extensively studied for biodegradable implant applications. Kannan (2010) reported that AZ91 sand-cast magnesium alloy has improved the degradation of magnesium by more than two times of magnitude. Walter and Kannan (2011) compared the *in vitro* degradation

behavior of pure magnesium, AZ91 magnesium alloy and a magnesium alloy containing rare-earth (Figure 2.1). They found that AZ91 magnesium alloy had the highest degradation resistance. Kirkland (2010) also reported that AZ91 magnesium alloy has the lowest degradation rate as compared to a wide range of other magnesium alloys.

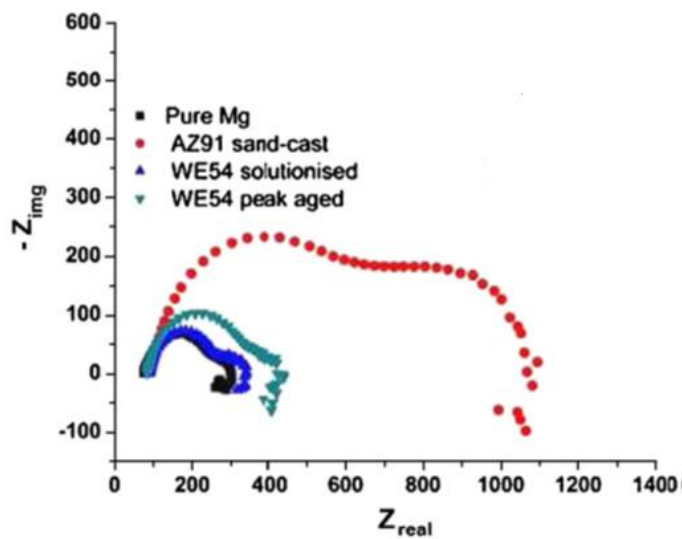


Figure 2.1 Nyquist plots of magnesium and its alloys in simulated body fluid (Walter and Kannan, 2011).

2.1.2.2 Coatings

Biocompatible coating is one of the most effective methods to control not only the general corrosion but also the localized corrosion of magnesium for biodegradable implant application. Biodegradable polymers are potentially successful coating materials for such applications due to their controlled degradation behavior and high biocompatibility. Bioceramics such as calcium phosphate and silicate are another class of materials that can also be coated onto magnesium-based materials for such applications.

2.2 Biodegradable Polymers

A polymer is a large molecule (macromolecule) composed of repeating structural units. These sub-units are known as monomers and are typically connected by covalent bonds. Biodegradable polymers such as polylactide acid (PLA) and polyglycolide acid (PGA) are a good choice of materials for temporary implant applications, since they degrade slowly in body fluid. In fact, synthetic polymers have received more attention for such application because of their versatility in the manufacturing process, their ability to change surface chemically and physically, and their ease of processing and high workability (Middleton and Tipton, 2000). Simple linear aliphatic polyesters such as PGA and PLA are popular and commercially available biodegradable polymeric biomaterials that have been used since 1960s as biodegradable sutures. PLA is a better choice than PGA, since the former degrades at a slower rate than the latter (Nair and Laurencin, 2007).

2.2.1 Polylactic Acid (PLA)

Polylactic acid (PLA) is a thermoplastic polymer, which is biodegradable and biocompatible. This polymer has been widely used in medical applications such as sutures, clips, plates and screws (Lunt, 1998). PLA is present in three isomeric forms d(-), l(+) and racimic (d, l). Both PDLA and PLLA are semi crystalline, with PLLA being the most popular form. It has a melting temperature of 173°-178°C and a glass transition temperature of about 60- 65°C. Poly (d, l- lactic acid) is amorphous with a glass transition temperature of 50- 60° C (Middleton and Tipton, 2000). However, the fact that these polymers possess poor mechanical properties as compared to that of natural bone, (Witte et al., 2008), is a major drawback for their potential use in implants

for load bearing orthopedic applications.. However, these polymers can be used as a successful coating material on magnesium-based alloys.

2.2.1.1 Degradation

PLA polymers are aliphatic polyesters due to the ester linkages in its backbone. The hydrolytic degradation of PLA occurs by the random chain scission of the ester groups as shown in Figure 2.2, accompanied by a reduction in the polymer molecular weight (Zhang et al., 1994; Lunt,1998). During the degradation, the PLA chain cleavage increases the number of carboxylic chain ends, which works to autocatalyze the ester hydrolysis (Ying-ying et al., 2006). It has been noted that the degradation of PLA film proceeds faster in the centre of the polymer film than on the surface. The degradation of PLA is through bulk erosion (Ying-ying et al., 2006; Nair and Laurencin et al, 2007).During the hydrolytic degradation, the fluid penetrates inside the polymer bulk. This catalyses the faster cleavage of the ester bond inside the polymer (Zhang et al., 1994). During the bulk degradation mechanism, the first change that can be observed is the molecular weight of polymer, which drops after the cleavage of the ester bond, followed in later stages by a decrease in the polymer weight and loss of its mechanical properties (Middleton and Tipton, 2000; Zhang et al., 1994). In general, the hydrolytic degradation of PLA is affected by the polymer crystallinity, the presence of catalysts and the location of the device (Lunt, 1998; Middleton and Tipton, 2000).

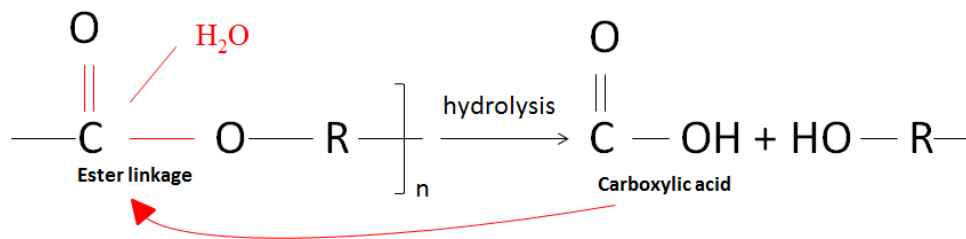


Figure 2.2 Bulk degradation of polylactic acid.

2.2.1.2 PLA on Magnesium

Chen et al (2011) coated PLA on pure magnesium and reported bulging of the coating after a period of exposure to simulated body fluid. They utilized a dip coating method for placing PLA on pure magnesium. Generally, the dip coating method produces a thick non-uniform coating. As a result, the coating's adhesion would not be appropriate and would perform poorly. Furthermore, the porosity/defects in dip coating are generally greater than in the spin coating method (Hong and Park, 2011). Thus, one could anticipate that a thin uniform coating on a magnesium alloy produced by the spin coating method would perform better than the alloy produced by the dip coating method. The former technique not only produces uniform coating with less porosity/defects, but also has good adhesion. Conversely, the dip coating method produces a relatively thick coating, which might provide high initial resistance but will peel off rapidly.

2.3 Plasma Electrolytic Oxidation

Plasma electrolytic oxidation (PEO), also known as micro arc oxidation (MAO), is a versatile and less expensive coating technique that was developed from a traditional anodic oxidation process. Generally, the PEO technique produces a uniform ceramic

coating with good adhesion (Yerokhin et al.,1999).There are many factors that can influence the PEO coating process, such as electrolyte composition, electrical parameters, oxidation time, and additives. They can affect the coating properties such as thickness, morphology and corrosion resistance.

2.3.1 PEO Coating Structure

Examination of the literature reveals that the PEO coating consists of mainly two layers, that is a top porous layer and an inner barrier layer. The inner layer is generally thin and adheres to the metal surface contributing strongly to the overall degradation resistance of the coating (Ghasemi et al., 2008; Liang et al., 2009). The surface of the PEO coating is generally rough, with a large number of pores. These pores are formed due to the co-existence of molten oxide and gas bubbles during the PEO coating process (Yerokhin et al., 1999). The major factors affecting the PEO coating morphology have been reported as the applied voltage and the electrolyte composition. Chasemi et al (2008) reported that high voltage promotes formation of a large size pores. Liang et al (2010) reported that the electrolyte composition could affect the structure of the PEO coating. For example, they observed that PEO film produced in a silicate based electrolyte had small-sized pores as compared to the film formed in a phosphate based electrolyte. They also reported that the PEO film thickness and roughness could be adjusted by changing the electrolyte composition. Another study, by Duan et al (2007), reported that the different morphology and film growth rate of PEO coating could be the result of metal reactivity with the electrolyte.

2.3.2 PEO on Magnesium

The PEO coating technique has been widely employed on magnesium and its alloys materials for improving their corrosion resistance for automobile applications (Duan et al., 2007; Liang et al., 2009; Ghasemi et al., 2008). Some of the key process parameters affecting the morphology of the coating, and hence the corrosion resistance of magnesium alloys, are listed in Table 2.2. Arrabal et al (2009) reported that the PEO coating on AZ91D alloy increased the corrosion resistance of the alloy in 3.5% NaCl significantly. The treated alloy reduced the corrosion current density by more than one order of magnitude more than the untreated alloy in a solution containing chloride. Another study by Wang et al (2009) showed that the silicate PEO coating also improved the corrosion resistance of AZ91 magnesium alloy: the i_{corr} was reduced by two orders of magnitude as compared to the untreated sample. Also, Chen et al (2007) reported that the PEO coating on AZ31 magnesium alloy improved the corrosion resistance by three times as compared to the base metal.

Table 2.2 Summary of PEO coatings on magnesium alloys

Alloy	Electrolyte	Conclusions	References
AM50 (4.4-5.5% Al, 0.26-0.6% Mn)	Coating : Silicate-PEO Coating solution: Na ₂ SiO ₃ (10g/l),KOH(1g/l) Corrosion solution: 0.1 M NaCl	Silicate-PEO film had a lower thickness with smother surface than phosphate-PEO. Corrosion resistance of silicate-PEO was higher than phosphate-PEO.	Liang et al.,(2009)
AM50 (4.4-5.5% Al, 0.26-0.6% Mn)	Coating: Phosphate-PEO Coating solution: Na ₃ PO ₄ (10g/l),KOH(1g/l) Corrosion solution: 0.1M NaCl Coating: Silicate-PEO Coating solution: Na ₂ SiO ₃ (10g/l),KOH(1g/l) Corrosion solution: (0.01M to 1M) NaCl	Increase in chloride concentration can accelerate the degradation. Si-PEO and P-PEO coatings performed poorly in high chloride concentrations.	Liang et al., (2010)
AM50 (5% Al, 0.5% Mn)	Coating: Phosphate-PEO Coating solution: Na ₃ PO ₄ (10g/l),KOH(1g/l) Corrosion solution: (0.01M to 1M) NaCl Coating: Silicate-PEO Coating solution: Na ₂ SiO ₃ (10g/l),KOH (10g/l) Corrosion solution: 0.1MNaCleffect of current density (15, 75, 150) mAcm ⁻²	Coating obtained at low current density showed highest corrosion resistance. Increase in current density increased the coating thickness, roughness and porosity level.	Srinivasan et al., (2009)
AZ91D (8.5-9.5% Al, 0,5-0.9% Zn,	Coating: Silicate-PEO Coating solution: Na ₂ SiO ₃ .9H ₂ O (10-20)g/l,KOH (3-8)g/l Corrosion solution: 3.5% NaCl Coating additive: Phosphate, borate and fluoride	The additive had a positive effect on the corrosion resistance of PEO. Borate and fluoride has the highest corrosion resistance.	Duan et al.,(2007)
AZ31 2.5-3.5%Al, 0.7-1.3% Zn)	Coating: Phosphate-PEO Coating solution: 30 g/l Na ₃ PO ₄ Corrosion solution: SBF Coating : effect of pulse frequency (300-3000)Hz	Better corrosion resistance was obtained by using a high pulse frequency.	Gu et al., (2012)

2.4 Calcium Phosphate

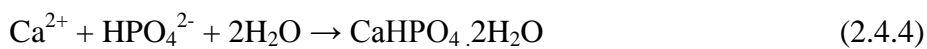
Calcium phosphate (CaP) is a bioceramic, which has been extensively studied for biomedical applications. It is biocompatible, possess high osteointegration, and degrades at a very slow rate (Kuo and Yen, 2002). Unfortunately, the brittleness and poor strength of CaP limit its use as a total implant material in load-bearing orthopedic applications (Groot et al., 1998). However, CaP has been successfully coated onto metallic implant materials such as stainless steel and titanium alloys (Kua and Yen, 2002; Liu et al., 2002).

2.4.1 CaP on Magnesium

The osteoconductivity of CaP and its slow replacement by the host bone (Shi, 2004), make it very attractive for coating on magnesium and magnesium alloy for biodegradable orthopedic implants. Different coating methods such as plasma spraying, sol-gel and physical vapour deposition have been tested for coating CaP on magnesium and its alloys. These methods are generally operated at high temperatures, which may potentially lead to chemical decomposition, thus resulting in non-uniform coating.

However, electrochemical deposition is a simple and inexpensive method, which is performed at room temperature and has a number of advantages. This technique can produce a uniform coating on complex shapes. Galvanostatic (constant-current density) and potentiostatic (constant-potential) are commonly employed methods for coating CaP on magnesium alloys. However, due to the hydrogen evolution during the coating process, these methods may create imperfections in the coating. The hydrogen bubbles could adhere to the metal surface, resulting in a non-uniform coating film with poor adhesion.

The electrochemical mechanisms of CaP formation are given in the equations below (Redepenning et al., 1996):



Pulse-electrodepositing, which involves an on-off cycle, is considered a potentially useful method for reducing the intensity of hydrogen evolution during the coating process (Chandrasekar and Pushpavanam, 2008). The on-off-cycle discharges the negatively charged layer and allows the ions to diffuse towards the substrate, which leads to a more even distribution of ions for coating. Wang et al (2010) studied HA coating using the pulse-electrodepositing method on Mg–Zn–Ca alloy. The test results showed that the coated material degraded at a slower rate. They also found that by regulating the pulse amplitude and width the HA coating achieved better adhesion. Another study by Kannan and Wallipa (2012) showed that the pulse-potential coating of calcium phosphate on AZ91 magnesium alloy exhibited ~3 times higher polarization resistance than that of the constant potential coating (Figure 2.3).

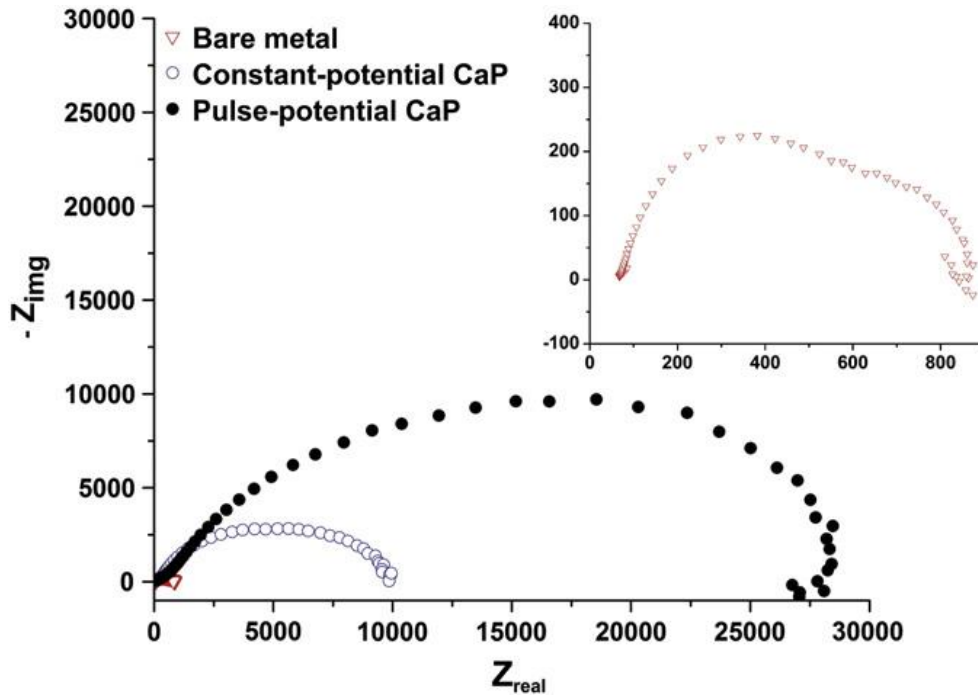


Figure 2.3 Nyquist plots of bare metal and the calcium phosphate coated magnesium alloy tested in SBF at 37 °C (Kannan and Wallipa, 2013).

Recently, a novel approach to decrease hydrogen bubble formation during the coating process was reported by Kannan (2012a). It was shown that by reducing the conductivity of the coating solution, the hydrogen bubble formation could be minimized. Ethanol was added to reduce the conductivity of the coating solution. The morphology of the coating produced in the conventional solution was significantly different from that produced with the addition of ethanol. While the conventional coating showed large clusters of particles, the coating produced with solution containing ethanol revealed a dense packing of particles. *In vitro* degradation test results showed that the conventional coating performed poorly, allowing SBF to permeate through the gaps between the particles, and as a result attacking the bare metal. Whereas, in the case of the coating created in the solution containing ethanol, the performance was significantly better. It was suggested that the denser packing of the coating significantly restricted the permeation of SBF through the coating. Kannan

(2012b) also evaluated the synergistic effect of pulse-method and ethanol addition to the coating solution on the coating formed on AZ91 magnesium alloy. Microstructures of the coating showed a closely packed morphology of the particles, resulting in superior performance under *in vitro* conditions.

The mechanical integrity of magnesium-based implants during service can be affected by their susceptibility to localized degradation. Areas subject to localized attack can act as stress concentrators and could cause the material to fail during loading. Unfortunately, magnesium and its alloys are susceptible to stress corrosion cracking in a chloride-containing environment (Kannan and Dietzel, 2012). The mechanical integrity of bare magnesium metal will be affected because magnesium dissolves in body fluids, since the fluid contains a large number of chloride ions (Kannan and Raman, 2008b).

Wang et al. (2010) investigated the mechanical integrity of a HAP coating on Mg-Zn-Ca alloy using slow strain rate testing (SSRT) technique. The test results showed that the ultimate tensile strength and time of fracture for the coated alloy was superior to that of the uncoated samples. Kannan and Orr (2011) studied the mechanical integrity of HAP coated AZ91 magnesium alloy by exposing the sample to SBF for 5 days and then testing it using a universal testing machine. The HAP coated alloy showed a 20% improvement in mechanical strength as compared to the uncoated alloy. SEM micrographs of the fractured samples revealed that the uncoated alloy underwent highly localized degradation as compared to the HAP coated samples. It was found that the alloy coated potentiostatically at -2 V performed better than the -3 V coated alloy.

2.5 Electrochemical Corrosion Techniques

Techniques such as electrochemical impedance spectroscopy (EIS) and potentiodynamic polarisation are well known test methods for evaluating the corrosion behaviour of metals and alloys. These techniques provide information on the corrosion rate, passivation and the localized behaviour of metallic material (Fontana, 1987; Orazem and Tribollet, 1996).

2.5.1 Potentiodynamic Polarization Method

Potentiodynamic polarization is a popular technique used to measure the corrosion rate of metals and alloys. This technique also provides information on the passivation and localized corrosion behavior of metals and alloys in a given environment. In this method potential is applied and the resulting current is measured. The potential is applied at an optimal scan rate. In the anodic polarisation, the potential is swept through the anodic direction from the corrosion potential (E_{corr}) value, whereas in the cathodic polarisation the potential is swept through the cathodic direction from the E_{corr} . Passivation and pitting susceptibility of the material may be presented on an anodic polarisation curve. In the cathodic curve, cathodic reaction such as hydrogen evolution becomes dominant. A typical polarisation curve is shown in Figure 2.4. The intersection of the cathodic and anodic curves is known as the corrosion potential (E_{corr}). The extrapolation of the linear region, otherwise known as the Tafel region, provides an estimation of the corrosion current density (i_{corr}). The corrosion current is proportional to the corrosion rate CR of the metal.

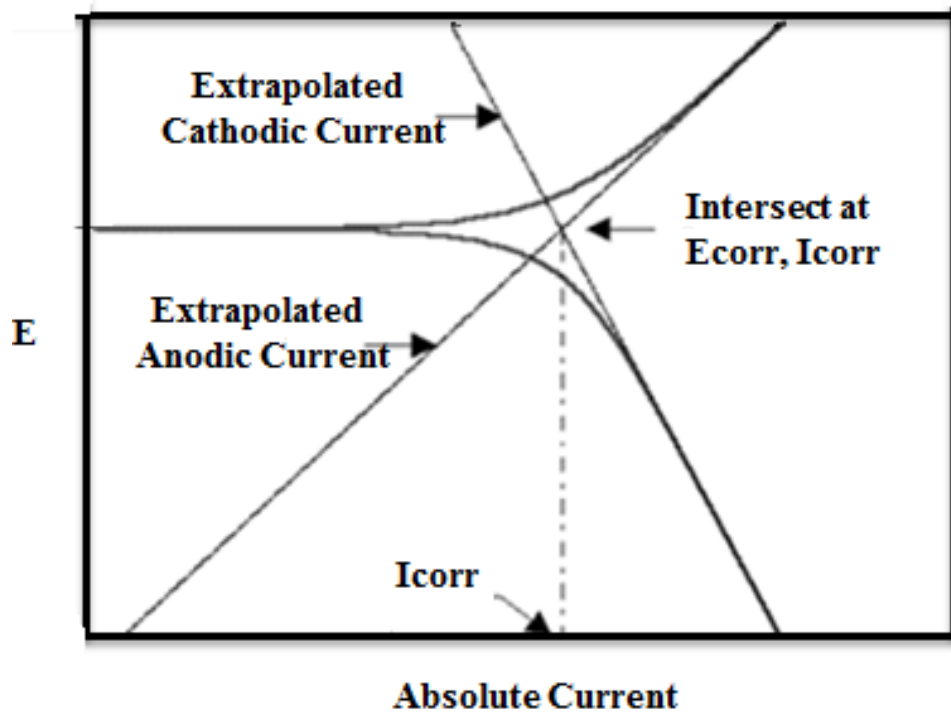


Figure 2.4 A typical potentiodynamic polarisation scan

2.5.2 *Electrochemical Impedance Spectroscopy (EIS)*

EIS is a non-destructive technique that can be used to study the corrosion behavior of metallic materials under long-term exposure. In this technique, a small excitation of AC potential between 5 to 50 mV is applied over a frequency range of 0.001 Hz to 100.000 Hz.

The response of the testing is an AC current signal which can be analysed as sinusoidal function (Fourier series). The expression of the impedance in a form of an equation is shown below:

$$Z = \frac{E_t}{I_t} = \frac{E_0 \sin(\omega t)}{I_0(\omega t + \varphi)} = Z_0 \frac{\sin(\omega t)}{\sin(\omega t + \varphi)} \quad (2.5.1)$$

E_t – potential at time (t)

E_0 – amplitude of the signal

ω - radial frequency

I_t – current at time (t)

I_0 – current signal amplitude

φ - phase shift between current and potential

The equation can be further simplified as

$$Z(\omega) = \frac{E}{I} = Z_0 \exp(j\varphi) = Z_0(\cos\varphi + j\sin\varphi) \quad (2.5.2)$$

The above equation contains a real and an imaginary part, which can be presented as a Nyquist plot as shown in (Figure 2.5). The real and imaginary parts are plotted as X-axis and Y-axis, respectively.

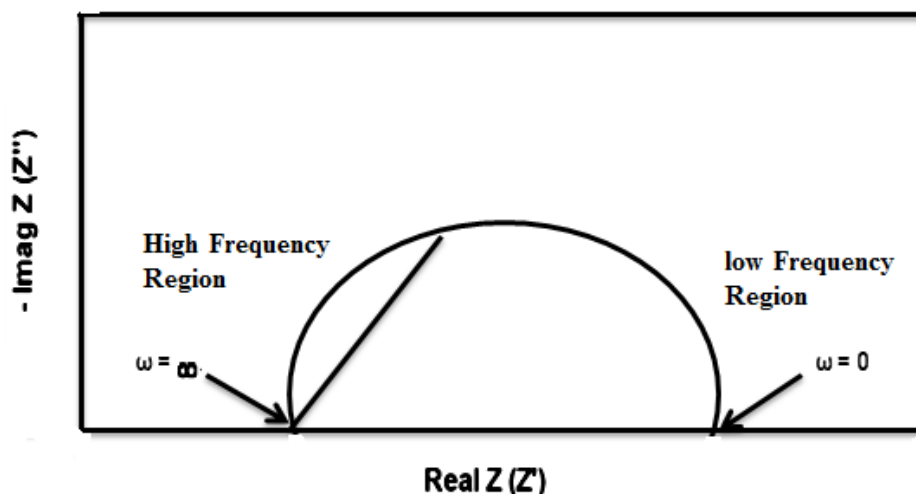


Figure 2.5 Atypical Nyquist plot

The Nyquist curves can generally be modelled and fitted with an equivalent circuit, based on the physical nature of the film formed on the metal or the corrosion phenomena. The quality of the curve fitting is judged by how well the fitting curve overlaps the original curve. A set of parameters is obtained from the fitting of the curve, which can be related to the electrochemical processes of the sample.

CHAPTER 3 MATERIALS AND EXPERIMENTAL PROCEDURE

3.1 Materials

In this study, pure magnesium (99.9 wt. %) and AZ91 (Al-9.18, Zn-0.78, Mn-0.20, Si-0.01, Fe-0.002, balance Mg, all wt%) have been used as the base materials.

3.2 Coatings

Prior to the coating, the samples (dimensions: 3 x 3 x 0.5 cm) were ground with SiC paper up to 320 grit and then ultrasonically cleaned in acetone and rinsed with ethanol.

3.2.1 Polymer Coating

Poly (L-lactide acid) PLLA, ester terminated RESOMER® L206 S (Aldrich), was used as a coating. The polymer was dissolved in dichloromethane (DCM) and the concentration of the polymer solution was in the range of 60–90 g/l. A spin coating method, as schematically represented in Figure 3.1, was used to coat the polymer. The spin coating was conducted in two steps, i.e., firstly a small amount of polymer solution was placed on the centre of the sample and then spin coated at 500 rpm for 10 sec. In the second step the coating was done at a rotational speed of 2000 rpm for 10 sec.

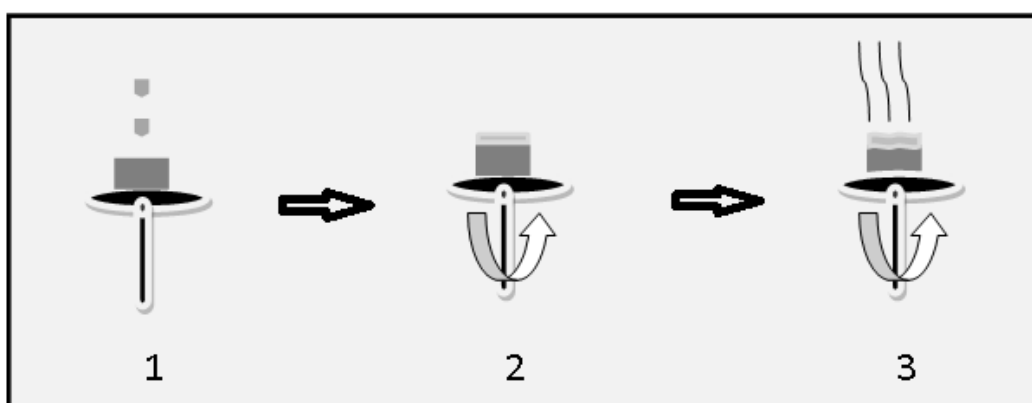


Figure 3.1 Schematic representation of the three-step spin coating method.

3.2.2 Plasma Electrolytic Oxidation (PEO) Coating

PEO coating was carried out in an electrolyte bath containing 2g/l KOH and 7g/l Na₂SiO₃. A pulsed constant current mode: 30mA/cm², 2ms/18ms pulse on/off time, was applied for 20 min with a final voltage of 483± 2V. Following the PEO coating, the samples were immersed in deionised boiling water for 90 min to remove the remains of the PEO coating solution and increase the compact inner layer thickness.

3.2.3 Calcium Phosphate (CaP) Coating

An electrodepositing method, with a typical three-electrode system, with sample as the working electrode, graphite as the counter electrode and Ag/AgCl as the reference electrode, was used to coat CaP on the samples. The coating solution consisted of 0.1 M Ca(NO₃)₂ and 0.06 M of NH₄H₂PO₄. A pulsed potential with -3V and a duty cycle of 35% for 60 min was applied for the coating.

3.2.4 Coating Characterization

The uniformity of the coatings was examined using scanning electron microscopy (SEM). A thickness gauge (Model: Dual Scope) was used to measure the coating thickness. Fourier transformed infrared spectroscopy (FTIR) analysis of the coatings was recorded in a spectral range of 1800-500 cm⁻¹ using a spectrometer (Model: Perkin Elmer spectrum 100).

3.3 In-vitro Degradation

In-vitro degradation studies were carried out in simulated body fluid (SBF) maintained at a physiological pH value of 7.4 and temperature of 37±0.5°C. The composition of the SBF is shown in Table 3.1. The SBF was buffered with tris (hydroxymethyl) aminomethane (TRIS) to maintain a physiological pH of 7.4. A standard three-electrode

system, as schematically shown in Figure 3.2, was used for the electrochemical tests (sample with 0.785 cm² exposed area as the working electrode, Ag/AgCl (saturated KCl) as the reference electrode and a graphite rod as the counter electrode). Measurements were taken using a VersaSTAT3 (PAR) potentiostat and a frequency response analyser. Electrochemical impedance spectroscopy (EIS) experiments were performed at the open circuit potential with AC amplitude of 5 mV over the frequency range of 10⁵ Hz to 10⁻² Hz. The EIS plots were modeled using ZSimpWin3.21 software. The post-degradation analysis was carried out using a scanning electron microscopy (SEM) Model: Jeol JSM 530LV to identify the mode of attack.

Table 3.1 Chemical composition of the simulated body fluid.

Reagent	Amount (1L)
NaCl (g/l)	8.036
NaHCO ₃ (g/l)	0.352
KCl (g/l)	0.225
K ₂ HPO ₄ ·3H ₂ O(g/l)	0.230
MgCl ₂ ·6H ₂ O (g/l)	0.311
1.0 M HCl (ml/l)	40
CaCl ₂ (g/l)	0.293
Na ₂ SO ₄ (g/l)	0.072
TRIS buffer(g/l)	6.063

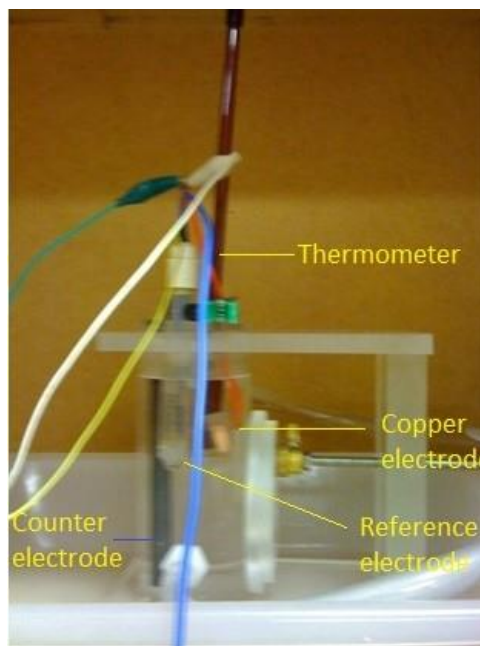
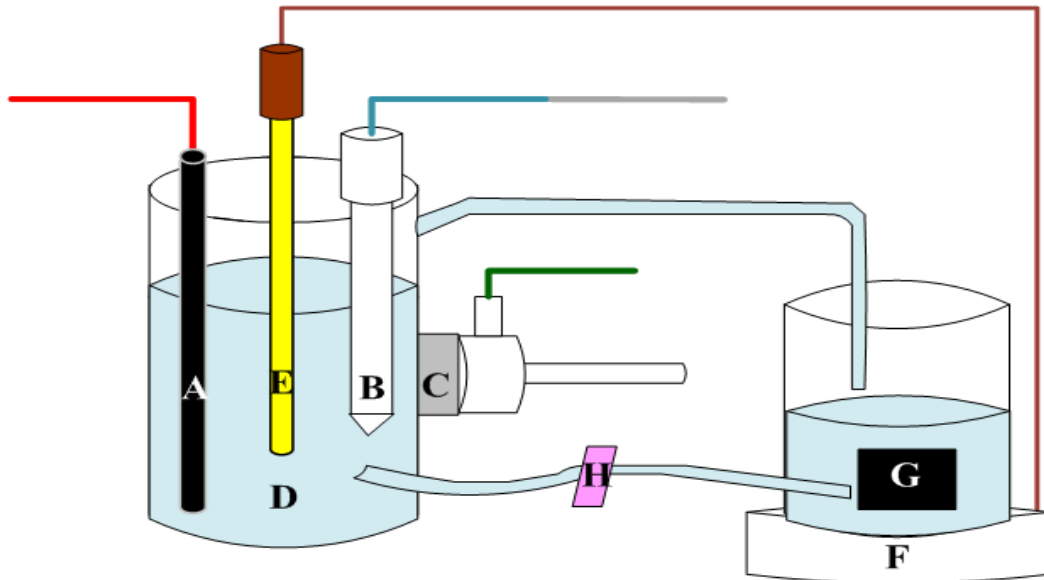


Figure 3.2 (a) Schematic and (b) photograph of the three-electrode cell used for *in vitro* degradation experiments.

(Note: A-graphite electrode; B-reference electrode; C-working electrode; D-SBF; E-temperature sensor; G-pump; H- SBF flow adjuster; F-hot plate)

CHAPTER 4 SINGLE LAYER COATINGS

In this chapter, the coating of polymer and/or ceramic materials on magnesium-based samples and their *in vitro* degradation behavior in simulated body fluid (SBF) are discussed.

4.1 Polymer Coating

A magnesium alloy, AZ91, was coated with PLA using the spin coating technique, and the *in vitro* degradation behavior of the coated alloy was analysed using electrochemical impedance spectroscopy (EIS) technique.

4.1.1 EIS Degradation

Figure 4.1 shows the Nyquist plots of the bare metal and PLA coated samples exposed to SBF. The bare metal exhibited two capacitive loops: one at high frequency range and another at mid-frequency range. The high frequency capacitive loop corresponded to the charge transfer resistance, and the second mid frequency capacitive loop corresponded to relaxation of mass transport through the corrosion product layer (Zucchi et al., 2006; Guo et al., 2005). This phenomenon suggested that the bare metal was only partially protected in SBF. At low frequency range, the bare metal revealed an inductive loop, which indicated that the alloy underwent pitting corrosion (Walter and Kannan, 2011; Jin et al., 2007). However, the PLA coated samples showed a large capacitive loop. A closer look at the high frequency region of the PLA coated samples revealed a small capacitive loop. Literature suggests that for polymer coated materials, a small capacitive loop at a high frequency region is attributed to the coating and a large capacitive loop at a mid-frequency region is a result of electrochemical processes occurring underneath the coating (Magalhaes et al., 1999). Interestingly, there was no sign of inductive loop for the PLA coated samples, which indicates that the polymer has

protected the alloy from pitting corrosion. Thus, it can be suggested that the polymer coating has prevented the permeation of chloride ions. Further, there was no indication of bulging of the coating, which suggests that the electrolyte permeation through the polymer was minimal.

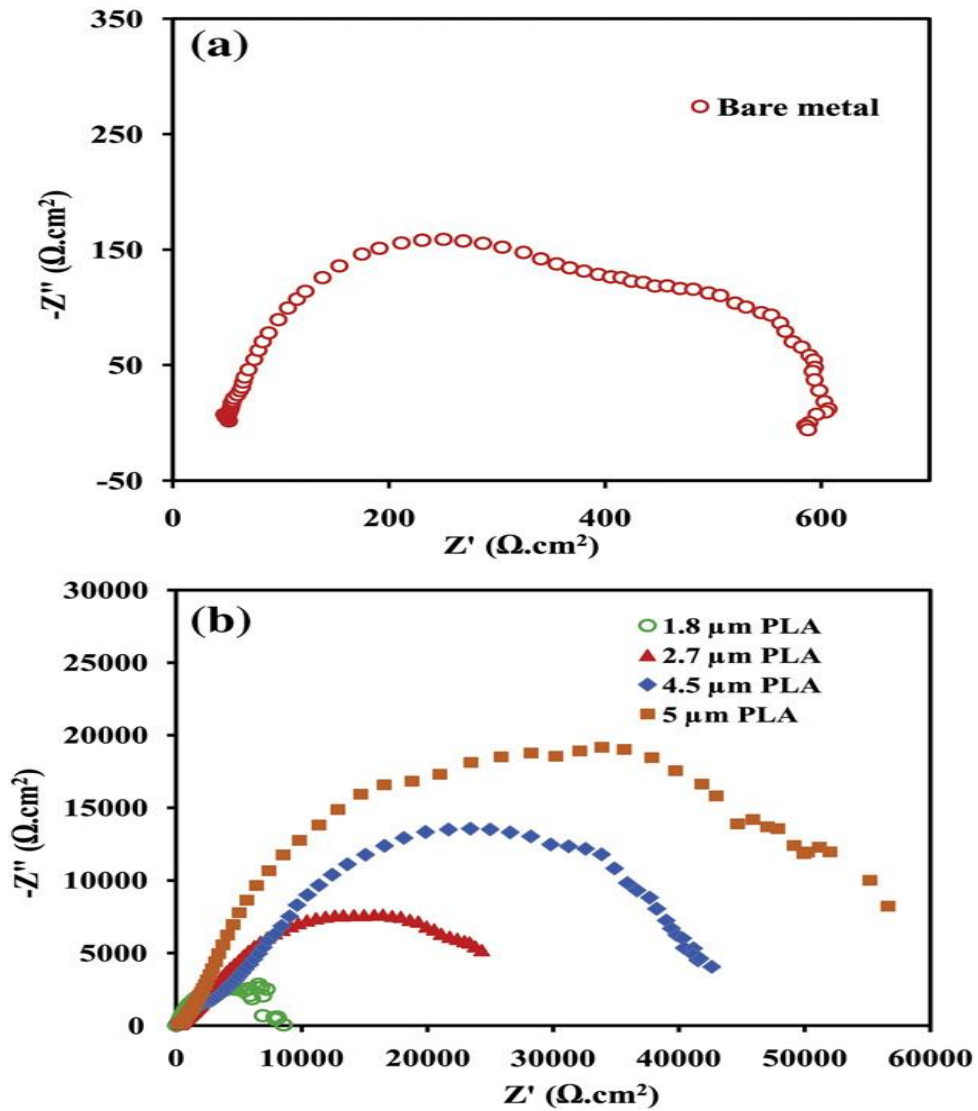


Figure 4.1 Nyquist plots of: (a) AZ91 magnesium alloy, and (b) PLA coated magnesium alloy samples, after a 2 h immersion in SBF.

The EIS spectra of the bare metal and the PLA coated samples were modeled using the equivalent circuits (Walter and Kannan, 2011; Chung et al., 2000; Kannan and Liyanaarachchi, 2013) shown in Figure 4.2, where R_s is the solution resistance, R_{L1} is

the pore resistance, R_{L2} is the layer resistance and R_{ct} is the charge transfer resistance. Q_{L1} , Q_{L2} and Q_{dl} are the constant phase elements that correspond to the PLA film, the alloy passive film and the electrical double layer, respectively. The polarization resistance (R_p) of the bare metal was obtained by adding R_{L2} and R_{ct} . The base metal showed R_p value of $475 \Omega \cdot \text{cm}^2$. In the case of the PLA coated samples, the R_p values were obtained by adding R_{L1} , R_{L2} , and R_{ct} .

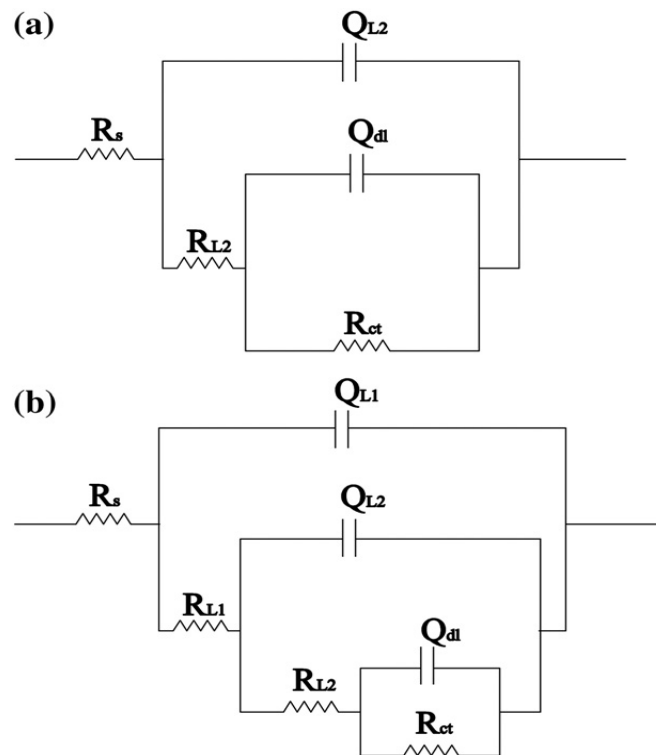


Figure 4.2 Equivalent circuits used for modelling EIS spectra of (a) AZ91 magnesium alloy and (b) PLA coated magnesium alloy samples, obtained after a 2 h immersion in SBF.

The R_p values of the PLA coated samples are plotted in Figure 4.3. It is clearly evident that PLA coating significantly increased the degradation resistance of the alloy, e.g., $1.8 \mu\text{m}$ PLA coating on the alloy showed a R_p of $9.5 \times 10^3 \Omega \cdot \text{cm}^2$, which is more than an order of magnitude higher than that of the bare metal. As the PLA film thickness increased, the degradation resistance of the alloy also increased significantly, e.g., $5 \mu\text{m}$

PLA coating showed a R_p of $6 \times 10^4 \Omega \cdot \text{cm}^2$, which is ~ 6 times higher than that of $1.8 \mu\text{m}$ PLA coating. Unfortunately, the increase in the PLA film thickness decreased the adhesion of the coating. The PLA coating with film thickness $\sim 2\text{--}3 \mu\text{m}$ showed good adhesion.

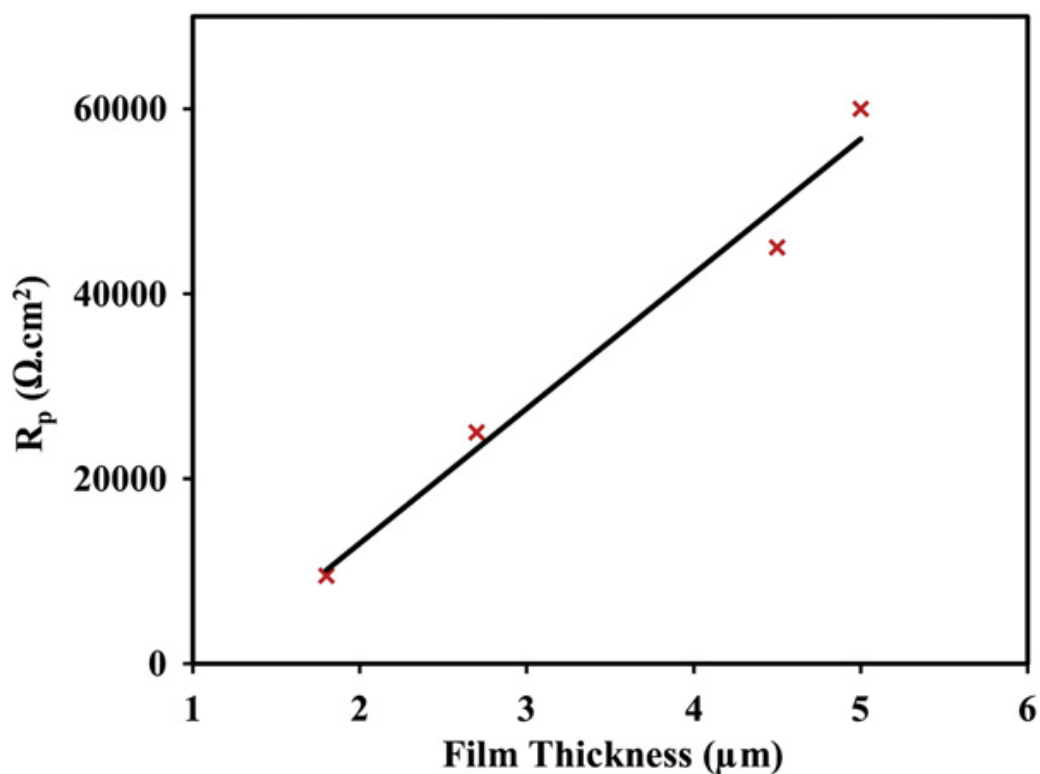


Figure 4.3 Polarization resistance (R_p) of PLA coated (different thickness) alloy samples after a 2 h immersion in SBF (All experiments were conducted in triplicate).

4.1.2 EIS Long-term Degradation

The long-term degradation behavior of the bare metal and the PLA coated samples (which showed good film adhesion) were studied using EIS at different exposure intervals. The R_p values of the bare metal and the PLA coated samples at different time intervals are shown in Figure 4.4. By increasing the SBF exposure time, the degradation resistance of the PLA coated samples gradually decreased. The literature suggests that PLA absorbs electrolyte (water) slowly, which fragments the ester backbone randomly; the mechanism is called bulk degradation (Nair and

Laurencin,2007; Zhang et al.,1994). Accordingly, the degradation resistance of the PLA coated alloy decreased gradually with the increase in exposure time. Photographs (Figure 4.4) of the bare metal and the PLA coated alloy after a 48 h exposure clearly indicate that the bare metal has undergone high degradation, whereas the PLA coated alloy shows only a slight degradation. It was also noted that, even after the 48 h exposure period, the PLA coating did not peel-off. The better performance of the PLA coated samples observed in this study, as compared to that of Chen et al. 2011, can be attributed to the thin coating produced by the spin coating method. This method produced better adhesion and possibly less porosity and defects. Interestingly, the bare metal showed a slight increase in the R_p with the increase in SBF exposure time. This could be due to the pseudo-passivation of the alloy in SBF. The higher degradation resistance of the base metal (AZ91 alloy), as compared to the pure magnesium, has also played a critical role in the better performance of the PLA coated alloy in this study.

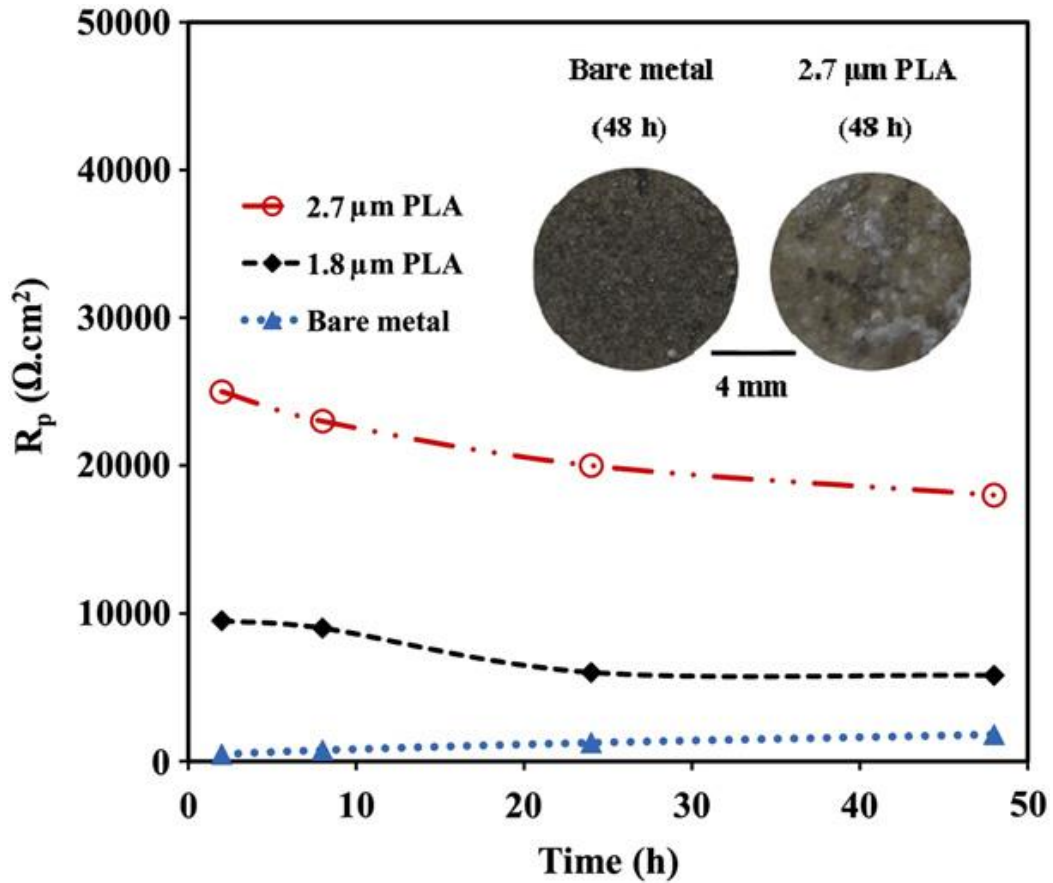


Figure 4.4 Polarization resistance (R_p) of AZ91 magnesium alloy and PLA coated magnesium alloy samples, after different immersion intervals in SBF.

4.2 PEO Coating

A silicate-based PEO coating was applied to pure magnesium using a pulsed constant current method. The morphology of the coating was analysed and the *in vitro* degradation behavior of the coated samples were evaluated.

4.2.1 Coating Morphology

The pulsed constant current PEO coating technique produced a coating thickness of $24 \pm 3 \mu\text{m}$ on the pure magnesium. Figure 4.5, shows the SEM micrographs of the PEO coating. The morphology of the coating reveals pores of two sizes (~ 5 and $2 \mu\text{m}$). Comparing the pulsed constant voltage mode work reported by Gu et al., 2011, the density of pores is relatively low in the pulsed constant current sample. A closer look at

the pores of the pulsed constant current sample (Figure 4.5b) indicates that they do not connect directly to the base metal. The literature also states that PEO coatings typically contain a compact inner layer and a porous outer layer (Ghasemi et al., 2008; Srinivasan et al., 2009). However, the reported interface or barrier layer is thin and composed out of MgO, regardless of the electrolyte used (Blawert et al., 2012). A few fine cracks were observed in the coating (Figure 4.5b), which indicates the brittleness of the coating.

4.2.2 EIS Degradation

The Nyquist plots of the pure magnesium and the PEO coated magnesium are shown in Figure 4.6. As expected, the pure magnesium exhibited two capacitive loops and one inductive loop, suggesting the poor passivation tendency and pitting corrosion susceptibility of magnesium (Walter and Kannan, 2011). However, the PEO coated magnesium showed only one capacitive loop, which indicates the resistance of the coating.

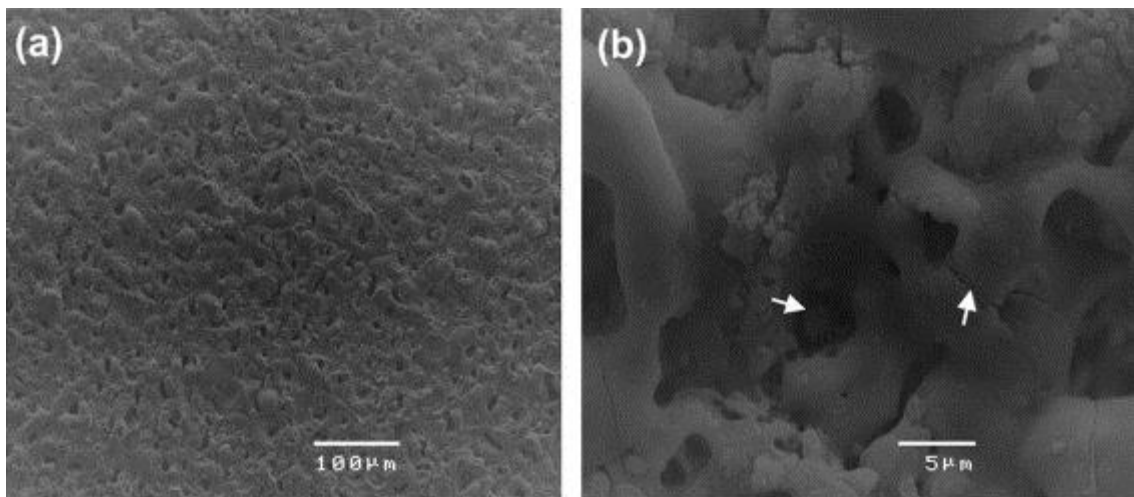


Figure 4.5 SEM Micrographs of PEO coating on pure magnesium: (a) low magnification and (b) high magnification.

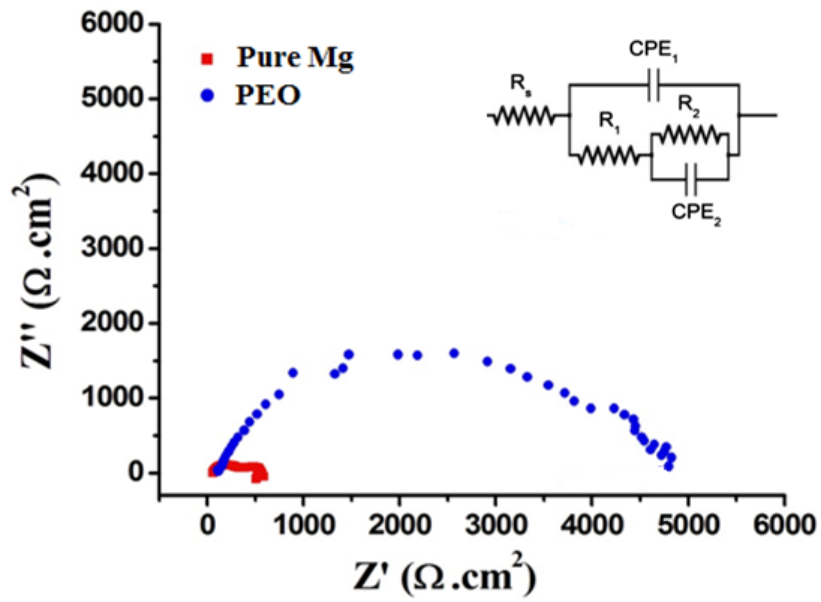


Figure 4.6 Nyquist plots of pure magnesium and PEO coated magnesium exposed to SBF.

The equivalent circuit used to model the impedance data is embedded in Figure 4.6 and the results obtained are given in Table 4.1. The model used in this study has been previously used for both bare magnesium alloys (Walter and Kannan, 2011) and PEO coated magnesium (Liang et al., 2009; Ghasemi et al., 2008; Srinivasan et al., 2009). Although an equivalent circuit was used for both the coated and the uncoated samples, the physical process represented by each element in the circuit is different, with the exception of the solution resistance R_s . For pure magnesium, R_1 represents the charge transfer resistance, CPE_1 the double layer capacitance, while R_2 and CPE_2 represent the film effects. For the PEO coated sample, R_1 and CPE_1 represent the outer porous layer, whereas R_2 and CPE_2 represent the resistance of the compact inner layer. For both pure magnesium and the PEO coated samples, the polarization resistance (R_p) was calculated by adding R_1 and R_2 . The R_p value obtained for pure magnesium was $480 \pm 72 \Omega \text{ cm}^2$, and for the PEO coated magnesium the R_p value was $4300 \pm 150 \Omega \text{ cm}^2$. It can be seen

in Table 4.1 that for the PEO coating, the porous layer resistance (R_1) is significantly smaller compared to the compact layer/inner barrier layer resistance (R_2). This suggests that the protection of the PEO coating in SBF critically depends on the compact inner layer. It has been reported that when the chloride concentration in the electrolyte increased, the pore resistance rapidly decreased, reaching a very low value over time and becoming insignificant as compared to the compact layer resistance (Liang et al., 2010).

Table 4.1 EIS fitting results for pure magnesium and PEO coated samples exposed to SBF.

Sample	CPE_1 ($\Omega^{-1} \cdot \text{cm}^{-2} \cdot \text{s}^{-n}$)	n	R_1 ($\Omega \cdot \text{cm}^2$)	CPE_2 ($\Omega^{-1} \cdot \text{cm}^{-2} \cdot \text{s}^{-n}$)	N	R_2 ($\Omega \cdot \text{cm}^2$)	R_p ($\Omega \cdot \text{cm}^2$)
Pure Mg	$4.8 (0.3) \times 10^{-5}$	0.82	411 (72.7)	$2.9 (0.2) \times 10^{-3}$	0.98	56.92 (0.59)	470 (72)
PEO	$1.06 (0.4) \times 10^{-8}$	0.98	88.2 (2.6)	$6.2 (1.7) \times 10^{-6}$	0.72	4211(147)	4300 (150)

Note: All experiments were conducted in triplicate and the standard deviations are provided in brackets

4.2.3 Potentiodynamic Polarization

The polarization curves of pure magnesium and the PEO coated magnesium are shown in Figure 4.7. The corrosion current (i_{corr}) for the PEO coated magnesium was 65% less than that of pure magnesium, i.e., $i_{\text{corr}} = 23.5 \pm 3.6 \mu\text{A}/\text{cm}^2$ for pure magnesium and $i_{\text{corr}} = 8.3 \pm 3 \mu\text{A}/\text{cm}^2$ for the PEO coated magnesium. The passivation potential range for PEO coated magnesium (400mV) was higher than that for pure magnesium (300mV). Interestingly, both the samples showed a similar breakdown potential (-1.5V), which indicates that the nature of the protective film is similar, i.e., MgO and/or Mg(OH)₂.

Thus the major positive effect of the PEO coating was due to the significant reduction in the cathodic activity as compared to the anodic behavior.

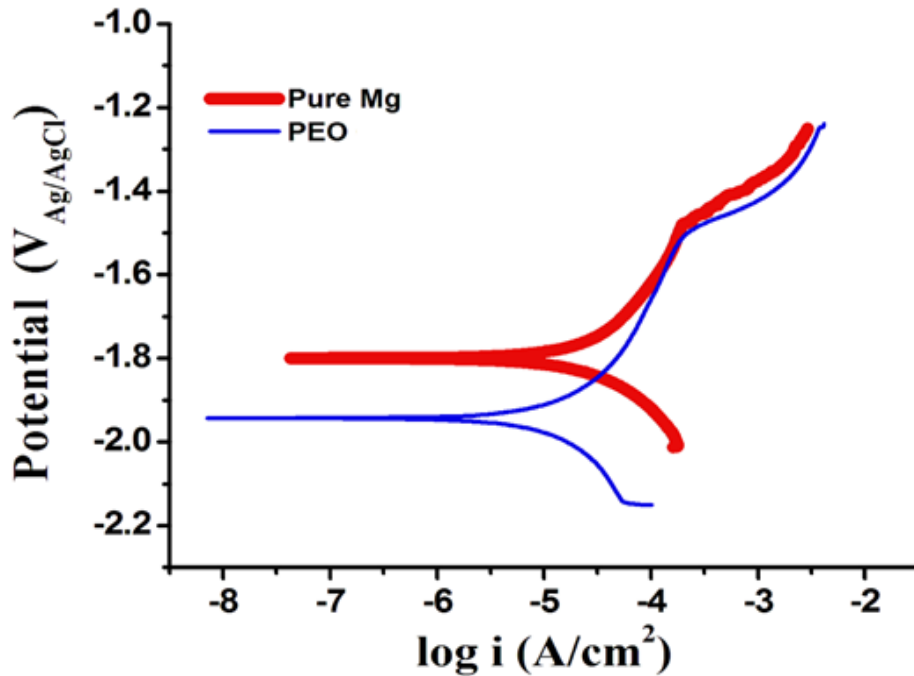


Figure 4.7 Potentiodynamic polarisation plots for the pure magnesium and PEO coated magnesium exposed to SBF.

4.2.4 Post-degradation Analysis

Figure 4.8 (a, b) shows the post-degradation SEM micrographs of pure magnesium and the PEO coated magnesium. Pure magnesium, as expected, exhibited a large number of pits (Figure 4.8a). A higher magnification view of the sample revealed mud-cracking (degradation product cracking) throughout the sample (Figure 4.8b). However, the PEO coated sample did not show any significant attack (Figure 4.8c). Only a few areas exhibited some degradation, and clearly no pitting attack was seen in the PEO coated sample. A closer look at the attacked regions (Figure 4.8d) revealed degradation along the fine cracks, however it was minimal. However, the degradation behavior of the pulsed constant current method cannot be directly compared with the pulsed constant

voltage method of coating by Gu et al. (2011), since the latter has not been evaluated by electrochemical methods. It is important to note that the pulsed constant current method PEO coating produced in the work did not show any significant localized degradation such as pitting even after the material was polarized.

XRD analysis of the PEO coating before and after exposure to the SBF shown in Figure 4.9 revealed that, besides the coating components, Mg_2SiO_4 and MgO , $\text{Mg}_2\text{PO}_4\text{OH}$ and $\text{Ca}_3(\text{PO}_4)_2$ were present after the immersion in SBF. This indicates that the porous top-layer is stable even after the short-term immersion in SBF. Also, it has contributed to the stability of the inner layer of the PEO coating and consequently to the overall degradation resistance of the alloy. The porous outer layer may have partially inhibited the free flow of aggressive ions towards the inner layer by promoting precipitation ($\text{Mg}_2\text{PO}_4\text{OH}$ and $\text{Ca}_3(\text{PO}_4)_2$) on the porous surface layer.

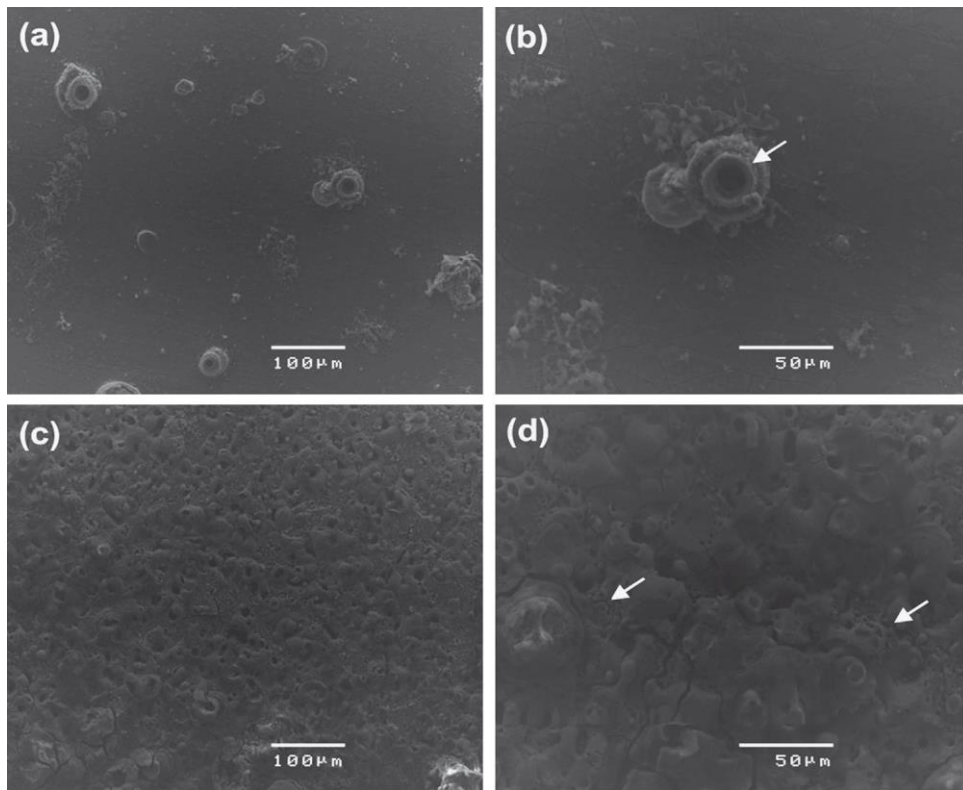


Figure 4.8 Post-degradation SEM micrographs of: (a,b) pure magnesium and (c,d) PEO coated magnesium

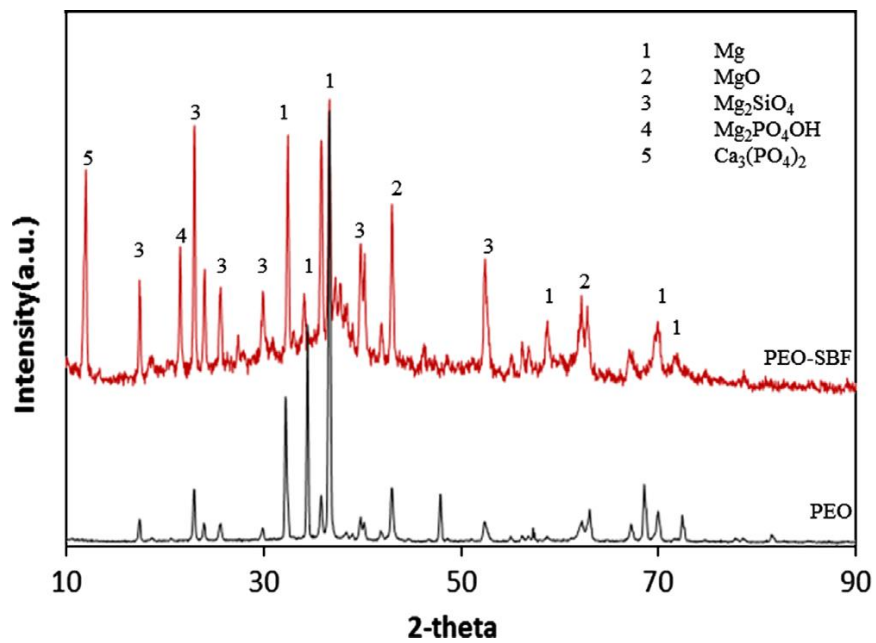


Figure 4.9 XRD spectra of PEO coated magnesium before and after exposure to SBF.

4.2.5 EIS Long-term Degradation

Long-term *in vitro* degradation studies were performed on the bare metal and the coated samples. The R_p values for the samples at different exposure times in SBF are shown in Figure 4.10. As the R_p of pure magnesium remained relatively stable at a low value ($\sim 1000 \Omega \cdot \text{cm}^2$), the R_p of the PEO coated samples decreased by 80% after 48h, from $4300 \Omega \cdot \text{cm}^2$ to $900 \Omega \cdot \text{cm}^2$. The drop in the R_p values suggests that the electrolyte has penetrated through the porous layer and attacked the base metal. Since the R_p of both bare metal and the PEO coated samples were similar and low after 48 h exposure, the experiments for these samples were stopped after 48 h.

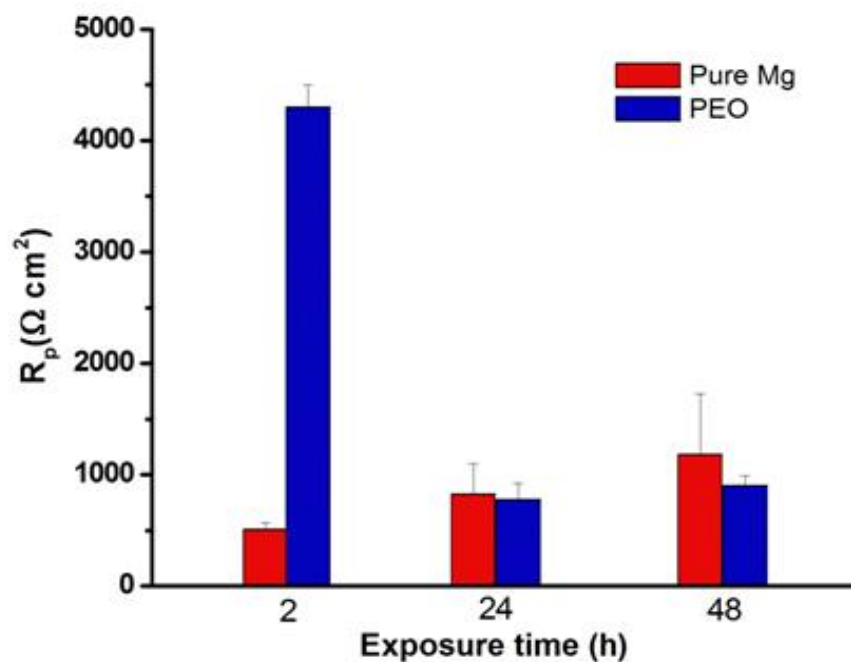


Figure 4.10 Polarization resistance (R_p) of pure magnesium and PEO coated samples after different immersion intervals.

4.3 Summary

The PLA coating on AZ91 magnesium alloy using spin coating method was shown to be beneficial for enhancing the degradation resistance of the alloy. The degradation

resistance of the alloy increased substantially with the increase in the coating thickness: 5 μm thick PLA coating showed more than two orders of magnitude higher polarization resistance than that by the bare metal. Unfortunately, the higher coating thickness resulted in poor adhesion. A thin film coating ($\sim 2\text{--}3\ \mu\text{m}$) on the alloy showed good adhesion and degradation resistance. Although the degradation resistance of the PLA coated samples decreased gradually with the increase in SBF exposure time, their degradation resistance was significantly higher than that of the bare metal, even after a 48 h exposure.

The pulse-current silicate-based PEO coating has significantly improved the degradation resistance of pure magnesium. The PEO coating increased the polarization resistance (R_p) of magnesium by an order of magnitude and reduced the corrosion current (i_{corr}) by 65 %. EIS modeling suggested that the inner compact layer resistance of the PEO coating was critical for the overall degradation resistance of the material.

CHAPTER 5 DUAL LAYER COATINGS

In order to further enhance the degradation resistance of the porous PEO coated magnesium, an additional coating was applied to seal the pores in the PEO coating. Two types of coating materials, i.e., polymer (PLLA) and ceramic (CaP), were used in this work.

5.1 Polymer Coating on PEO

PLLA was coated on a silicate-based PEO coating on pure magnesium. A two-step spin coating method was used for coating PLLA. A low-speed step was initially used to allow the polymer to permeate through the pores. Subsequently, a high-speed step was used to achieve a thin film on the PEO surface. The *in vitro* degradation behavior of the PEO-PLLA coated samples was evaluated using electrochemical techniques.

5.1.1 EIS *In-vitro* Degradation

The Nyquist plots for the pure magnesium and the coated samples after 2 h exposure in SBF are shown in Figure 5.1(a, b). The pure magnesium shows two capacitive loops and one inductive loop. In contrast to the pure magnesium, the PEO coated samples showed only one large capacitive loop. Interestingly, the PEO-PLLA coated samples showed two large capacitive loops. However, there was no inductive loop.

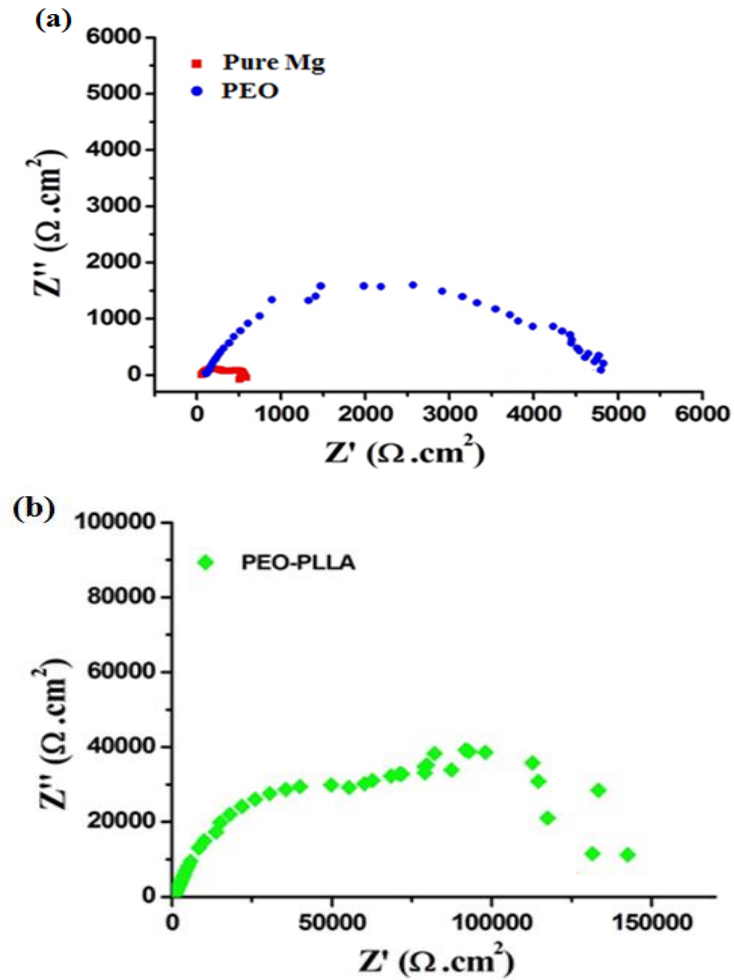


Figure 5.1 Nyquist plots of (a) pure Mg and PEO coated sample, and (b) PEO-PLLA coated sample, after 2 h immersion in SBF.

An equivalent circuit model: $R(Q(R(QR)))$, was used to analyse the impedance data. This model has been used for bare Mg (Walter and Kannan, 2011), PEO coated samples (Alabbasi et al., 2013; Liang et al., 2009; Ghasemi et al. 2008) and double-layered coated samples (Zeng et al., 2010). For pure magnesium, R_1 represents the charge transfer resistance, CPE_1 the double layer capacitance; R_2 and CPE_2 represent the film effects. For the PEO coated sample, R_1 and CPE_1 represent the outer porous layer, while R_2 and CPE_2 represent the resistance of the compact inner layer. For PEO-PLLA, the coated sample R_1 and CPE_1 represent the resistance of PLLA, while R_2 and CPE_2 represent the resistance of the PEO layer. The polarization resistance (R_p) was calculated by adding R_1 and R_2 .

Table 5.1 EIS fitting results for the pure magnesium, PEO coated and PEO-PLLA coated samples exposed for 2 h in SBF

Sample	CPE_1 ($\Omega^{-1} \cdot \text{cm}^{-2} \cdot \text{s}^{-n}$)	N	R_1 ($\Omega \cdot \text{cm}^2$)	CPE_2 ($\Omega^{-1} \cdot \text{cm}^2 \cdot \text{s}^{-n}$)	n	R_2 ($\Omega \cdot \text{cm}^2$)	R_p ($\Omega \cdot \text{cm}^2$)
Pure Mg	$4.8 (0.3) \times 10^{-5}$	0.82	411 (72.7)	$2.9 (0.2) \times 10^{-3}$	0.98	56.92 (0.59)	470 (72)
PEO	$1.06 (0.4) \times 10^{-8}$	0.98	88.2 (2.6)	$6.2 (1.7) \times 10^{-6}$	0.72	4211(147)	4300 (150)
PEO+PLLA	$1.31 (1.05) \times 10^{-6}$	0.61	1544 (339)	$4.2 (3.9) \times 10^{-7}$	0.81	117000 (28545)	118544 (26319)

Note: All experiments were conducted in triplicate and the standard deviations are provided in brackets

The results obtained from the EIS modeling are shown in Table 5.1. The PEO coated samples showed close to an order of magnitude higher R_p than the pure magnesium. Importantly, the PEO-PLLA coated samples showed close to three orders of magnitude higher R_p than the pure Mg and was close to two orders of magnitude higher R_p than the PEO coated samples. The R_p values were $470 \Omega \cdot \text{cm}^2$, $4300 \Omega \cdot \text{cm}^2$, and $1.18 \times 10^5 \Omega \cdot \text{cm}^2$ for the pure magnesium, the PEO coated and the PEO-PLLA coated samples, respectively. For both the PEO and the PEO-PLLA coated samples, the R_2 is significantly higher as compared with R_1 , which indicates that the R_p for both the coatings depends on the inner layer resistance.

5.1.2 Potentiodynamic Polarization

The polarization curves for the pure magnesium, the PEO coated and the PEO-PLLA coated samples are shown in Figure 5.2 and the corresponding electrochemical data are presented in Table 5.2. The E_{corr} of the PEO-PLLA coated samples shifted by $\sim 250\text{mV}$ toward the noble direction as compared to that of the pure magnesium, whereas the PEO coated samples showed a $\sim 100\text{mV}$ shift towards the active direction. The corrosion current density (i_{corr}) calculated based on the cathodic curves showed that the i_{corr} of the pure magnesium was reduced by 65% with the PEO coating and by almost 100% with the PEO-PLLA coating.

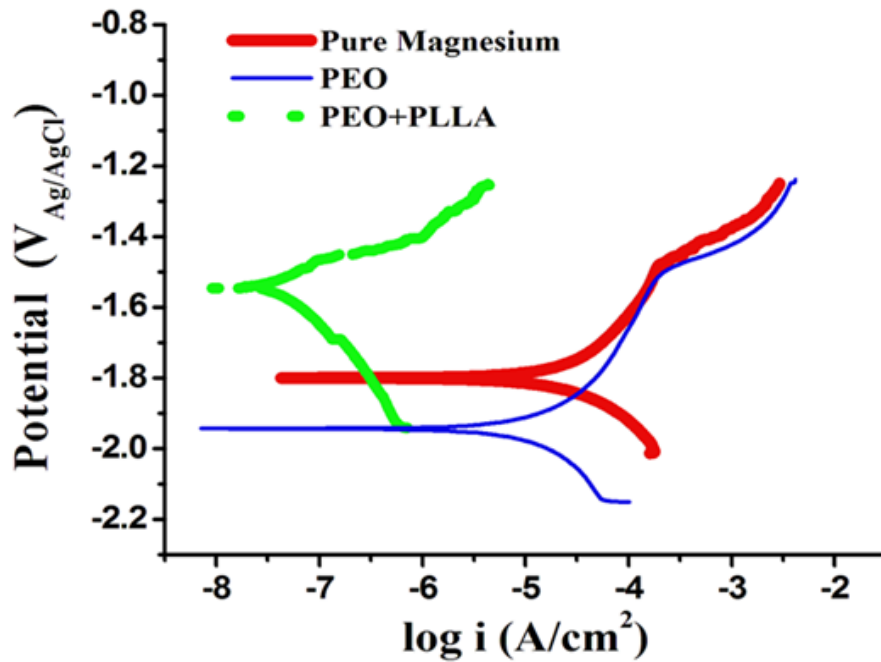


Figure 5.2 Potentiodynamic polarization curves of pure magnesium, PEO coated and PEO-PLLA coated samples after 2 h immersion in SBF.

Table 5.2 Electrochemical degradation data for pure magnesium, PEO coated and PEO-PLLA coated samples from potentiodynamic polarization curves

Sample	E_{corr} V _(Ag/AgCl)	i_{corr} ($\mu\text{A}/\text{cm}^2$)
Pure Mg	-1.8 (0.02)	23.5 (3.6)
PEO	-1.92 (0.02)	8.3 (3)
PEO-PLLA	-1.54 (0.01)	0.03 (0.2)

Note: All experiments were conducted in triplicate and the standard deviations are provided in brackets

5.1.3 EIS Long-term Degradation

Long-term *in vitro* degradation studies were performed on the bare metal and the coated samples. It should be noted that the SBF was changed after every 24 h exposure to maintain the pH at 7.4. The R_p values for the samples at different exposure times in

SBF are shown in Figure 5.3. As the R_p of pure magnesium remained relatively stable at a low value ($\sim 1000 \Omega \cdot \text{cm}^2$), the R_p of the PEO coated samples decreased by 80% after 48h, from $4300 \Omega \cdot \text{cm}^2$ to $900 \Omega \cdot \text{cm}^2$. The drop in the R_p values suggests that the electrolyte has penetrated through the porous layer and attacked the base metal. Since the R_p of both bare metal and the PEO coated samples were similar and low after 48 h exposure, the experiments for these samples were stopped after 48 h.

The PEO-PLLA coated samples also showed a drop in the R_p value after 24 h exposure; however, the R_p was more than one order of magnitude higher than that of the pure magnesium and the PEO coated samples. The decrease in the R_p of the PEO-PLLA coated samples could be attributed to the bulk degradation mechanism of PLLA (Zhang et al., 1994). It should be noted that the R_p value of the PEO-PLLA samples, even after 100 h exposure, was $5.4 \times 10^3 \Omega \cdot \text{cm}^2$, which is still significantly higher than that of the PEO coated samples measured after 48 h. The results suggest that the PLLA coating has filled the porous of the PEO layer and prevented the penetration of the electrolyte, and as a result the PEO-PLLA coated samples showed higher R_p than the PEO coated samples throughout the tests. Interestingly, the R_p reported by (Lu et al., 2011) for a PEO-PLA coated alloy was higher than that observed in this study. This could be due to the difference in the pH condition of the electrolyte during the experiments. If the electrolyte is not changed regularly during the long-term experiments, which was the case in the (Lu et. al., 2011), the pH of the electrolyte will increase. As a consequence, magnesium passives and the R_p would not change significantly or it might even increase. Hence, it is critical to change the SBF regularly during the long-term testing to maintain the pH of the electrolyte to mimic physiological conditions.

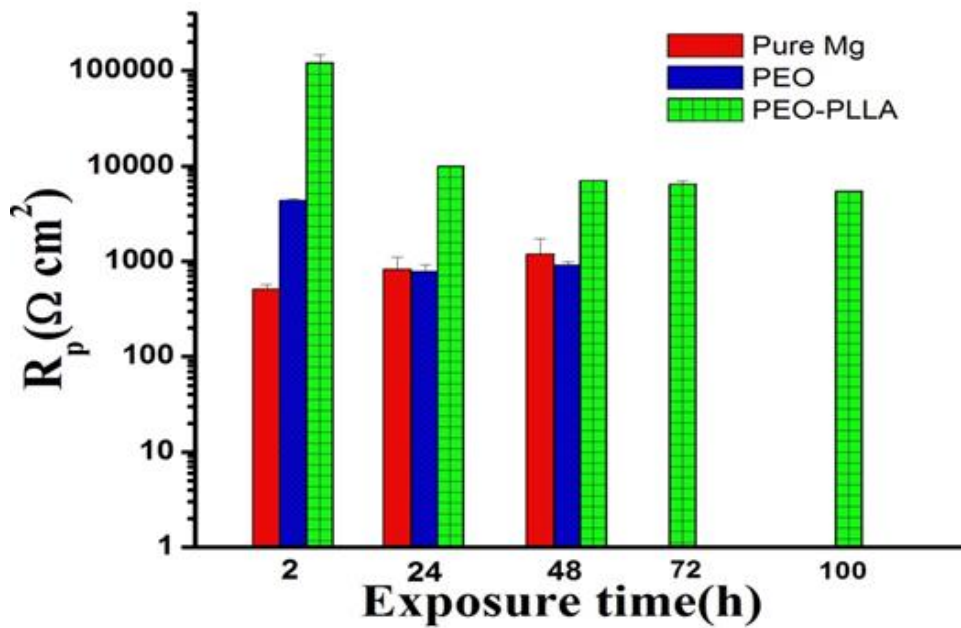


Figure 5.3 Polarization resistances (R_p) of pure magnesium, PEO coated and PEO-PLLA coated samples after different immersion intervals in SBF.

5.1.4 Post-degradation Analysis

Figure 5.4 shows the post-degradation photographs of the pure magnesium and the coated samples. The pure magnesium has undergone high degradation after 48 h exposure to SBF. Highly localized degradation is readily seen in the photograph of the pure magnesium. The PEO coated samples showed no highly localized degradation, but a few patches of localized attack were observed. In contrast to the pure magnesium and PEO coated samples, the PEO-PLLA coated samples showed no sign of localized degradation.

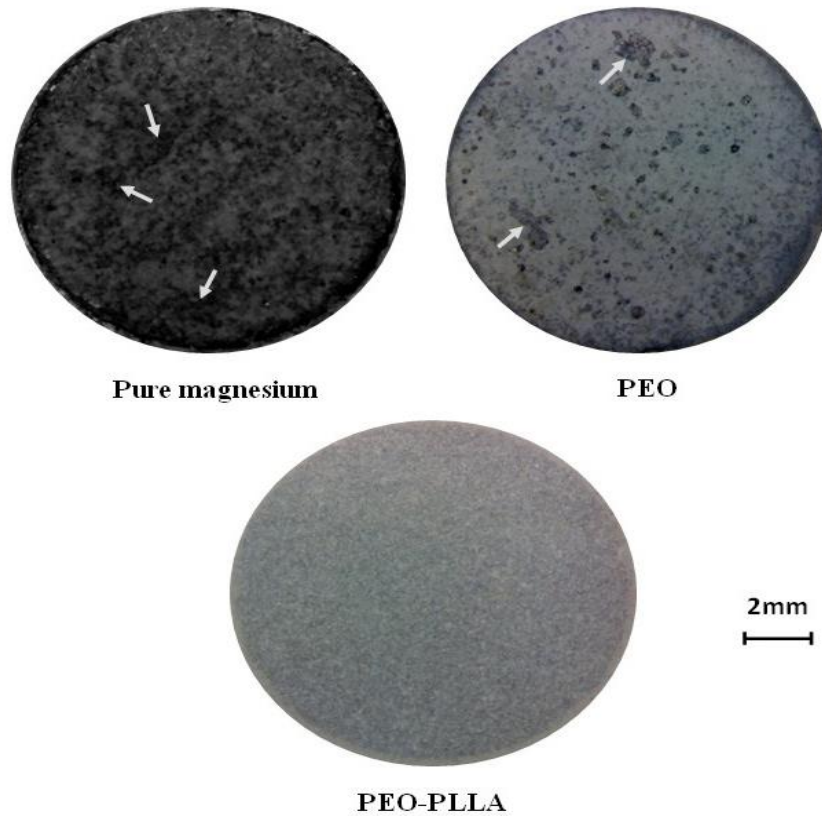


Figure 5.4 Photographs of pure magnesium and PEO coated sample after 48 h exposure in SBF, and PEO-PLLA coated sample after 100 h exposure in SBF

5.1.5 Degradation Mechanism

The degradation mechanisms of the pure magnesium, the PEO coated and the PEO-PLLA coated samples are schematically shown in Figure 5.5. It is well known that high-chloride concentration, as in the SBF, causes highly localized degradation in pure magnesium (Kannan, 2010). The native film (MgO) and the degradation product film, $\text{Mg}(\text{OH})_2$, formed in aqueous solution, are not protective in chloride-containing solution (Song and Atrens, 2003). As a result, a high level of localized degradation was observed within 48 h of exposure to SBF. The PEO coating did show some protection against degradation during the initial exposure period. However, the porous nature of the outer film allowed the chloride ions to penetrate through and dissolve the inner layer, which led to localized degradation after a period of exposure to SBF.

The double layer coating (PEO-PLLA) has shown a significant improvement in degradation resistance under short-term exposure. The polymer top layer has acted as a protective barrier, thus largely inhibiting the penetration of the electrolyte. With exposure time, polymer dissolution occurred and as a result of the bulk degradation mechanism of PLLA, the electrolyte has reached the porous layer and the base metal. Hence the resistance has decreased. However, the penetration of the electrolyte appears to be minimal since the R_p was significantly high even after 100 h exposure. It is important to note that there was no sign of localized degradation even after 100 h of exposure to SBF.

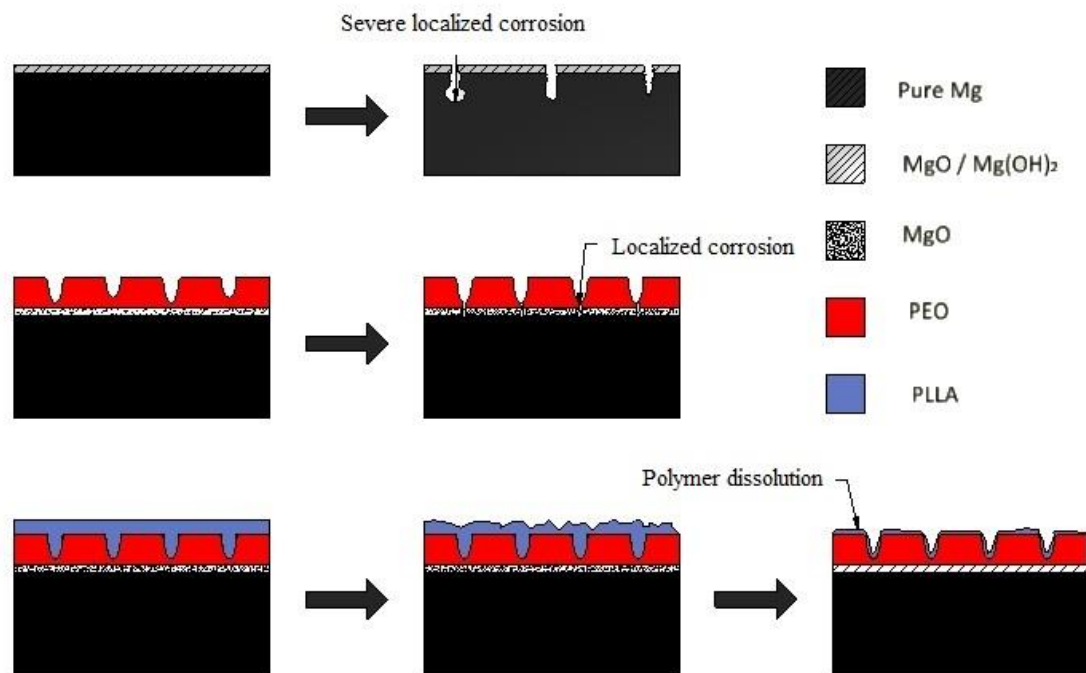


Figure 5.5 Schematic representations of the *in vitro* degradation processes of pure magnesium, PEO coated and PEO-PLLA coated samples.

5.2 Calcium Phosphate (CaP) Coating on PEO

CaP was coated on the PEO layer on pure magnesium using an electrochemical deposition method. The *in vitro* degradation behavior of the dual layer (PEO- CaP) coated material was tested using electrochemical methods in SBF.

5.2.1 Morphology

The SEM micrographs of the PEO and PEO-CaP coatings are shown in Figure 5.6 (a-d). The PEO coating exhibited a rough surface as shown in Figure 5.6a. A higher magnification of the coating revealed a porous structure (Figure 5.6b), which is expected for this method of coating. However, the PEO-CaP coating showed a flat morphology with some CaP particles protruding outside the surface (Figure 5.6c). A higher magnification revealed long thin CaP particles aggregated with small gaps (Figure 5.6d). However, there was no evidence of porosity in the underneath PEO layer, which suggests complete coverage of CaP coating. Coating thickness measurements showed that the thickness of the PEO coating was $24 \pm 3 \mu\text{m}$, and after the electrochemical deposition of CaP, the dual layer coating thickness was $37 \pm 4 \mu\text{m}$.

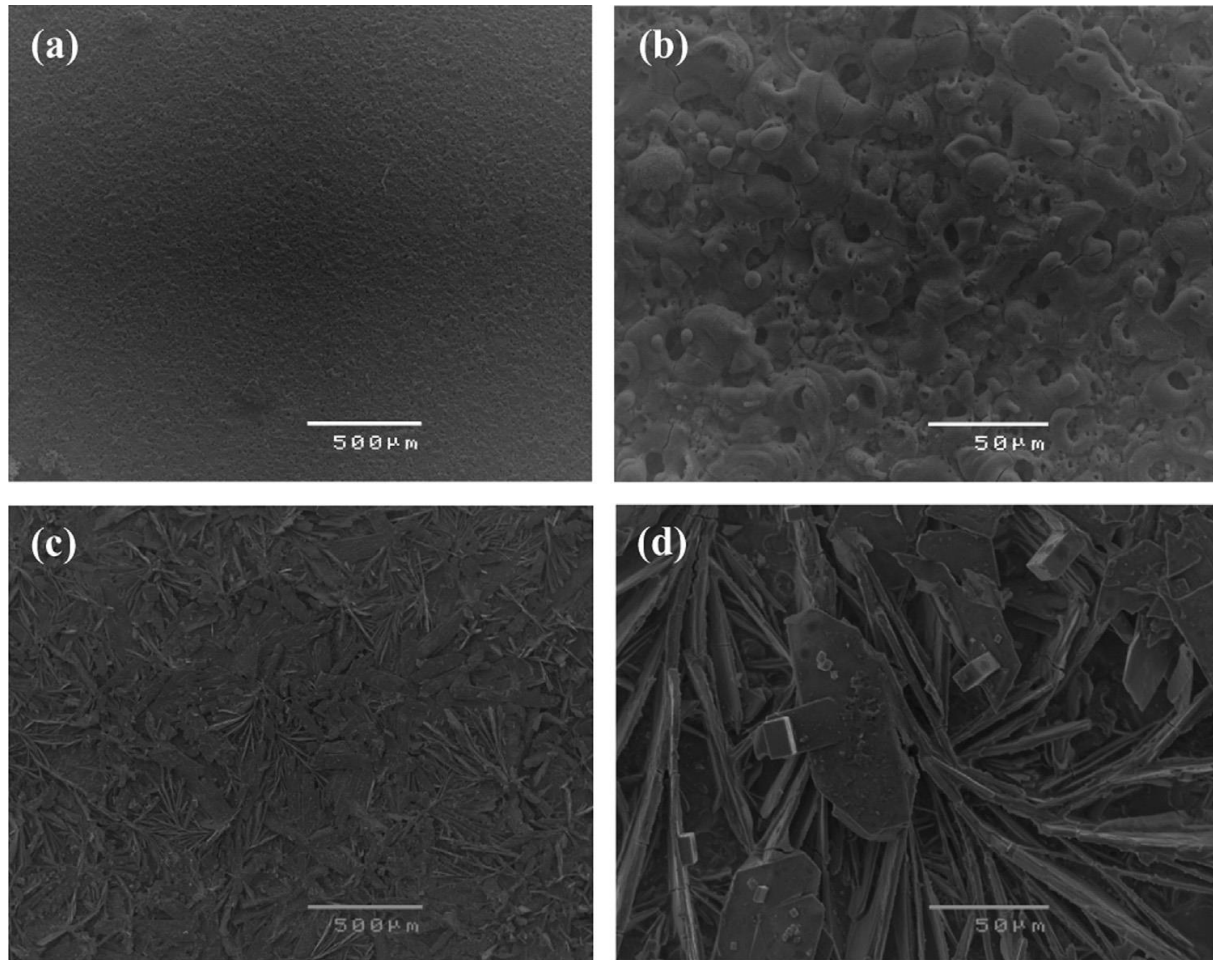


Figure 5.6 SEM micrographs of the coatings on pure magnesium: (a and b) PEO coating, and (c and d) PEO-CaP coating.

5.2.2 Coating Characterization

Figure 5.7 shows the FTIR spectra of PEO and PEO-CaP coated samples. The PEO coating showed strong peaks at 970 and 870 cm^{-1} corresponding to silicate (Beganskiene et al., 2004) and the PEO-CaP coating exhibited strong peaks at 1130, 1150 and 980 cm^{-1} corresponding to phosphate (Liu et al., 2011). The absence of silicate peaks for the PEO-CaP coated samples further confirms the tight coating of CaP. Based on previous work (Kannan and Orr, 2011), it can be suggested that the CaP coated formed is dicalcium phosphate dihydrate ($\text{CaHPO}_4 \cdot 2\text{H}_2\text{O}$).

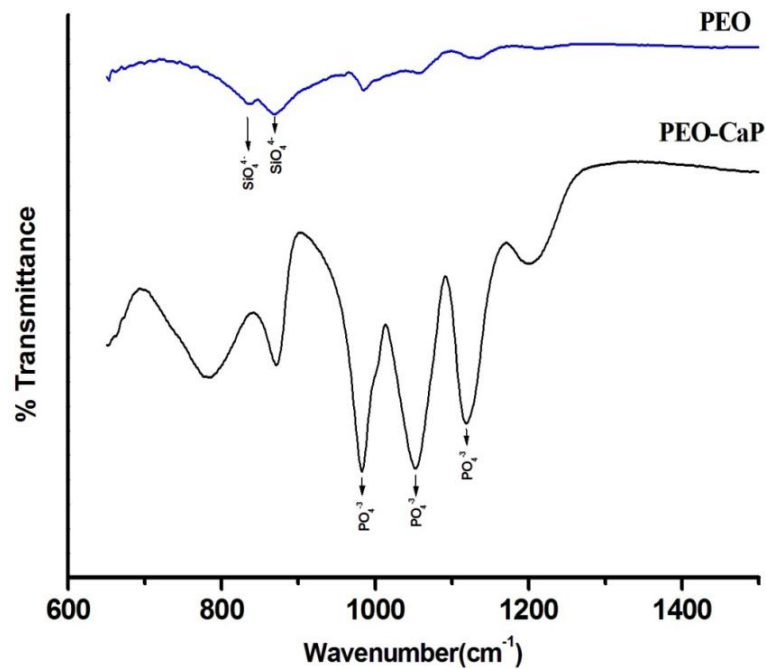


Figure 5.7 FTIR spectra of PEO and PEO-CaP coatings on pure magnesium.

5.2.3 EIS In-vitro Degradation

The Nyquist plots of the bare metal and the coated samples after 2 h exposure to SBF are shown in Figure 5.8. As expected, the pure magnesium, which is prone to general and localized degradation, showed two capacitance loops (one at high frequency and

another at a mid-frequency, suggesting partial protection) and an inductive loop at low frequency (indicating pitting corrosion) (Walter and Kannan, 2011; Jin et al., 2007). Both the coated samples (PEO and PEO-CaP), however, exhibited a large single capacitive loop suggesting a better performance of the material in SBF. Importantly, there was no sign of inductive loop for both the coated samples, which confirms that the samples did not undergo localized degradation. The polarisation resistance (R_p) of PEO-CaP coated metal was found to be approximately two orders of magnitude higher as compared to the pure Mg and one order of magnitude higher than that of PEO coated metal.

5.2.4 Potentiodynamic Polarization

The potentiodynamic polarization curves of the bare and the coated samples are shown in Figure 5.9 and the corresponding electrochemical data are listed in Table 5.3. Interestingly, the E_{corr} shifted by ~120 mV towards the active potential for PEO coated metal and the PEO-CaP coated metal shifted by 140mV toward the noble potential as compared to that of the pure magnesium. However, the corrosion current density (i_{corr}), calculated based on the cathodic curves, showed ~65% reduction with the PEO coating, and ~96% reduction with the PEO-CaP in comparison with that of the pure magnesium. Comparing the present study (PEO + cathodic deposition of CaP) with Liu et al.'s work, 2011 (PEO+ immersion coating of CaP), both on pure magnesium, it is evident that cathodically deposited CaP performs better than the CaP formed using the immersion method. The corrosion current (i_{corr}) for PEO+ CaP (cathodically deposited) on magnesium is ($i_{\text{corr}} = 5 \mu\text{A}$). Liu et al. observed ~50% decrease in the i_{corr} for PEO+ CaP as compared to PEO only, whereas the current study showed ~90% decrease for such comparison. This clearly suggested that cathodic deposition of CaP is more effective than immersion coating of CaP.

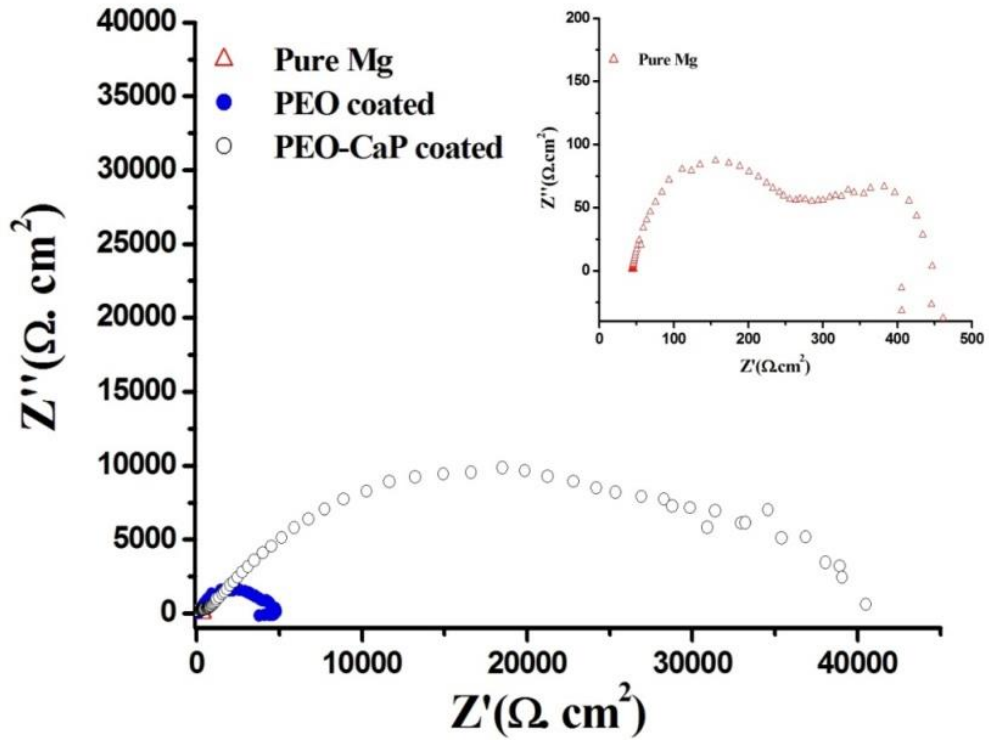


Figure 5.8 Nyquist plots of pure magnesium, PEO coated and PEO-CaP coated magnesium samples exposed to SBF

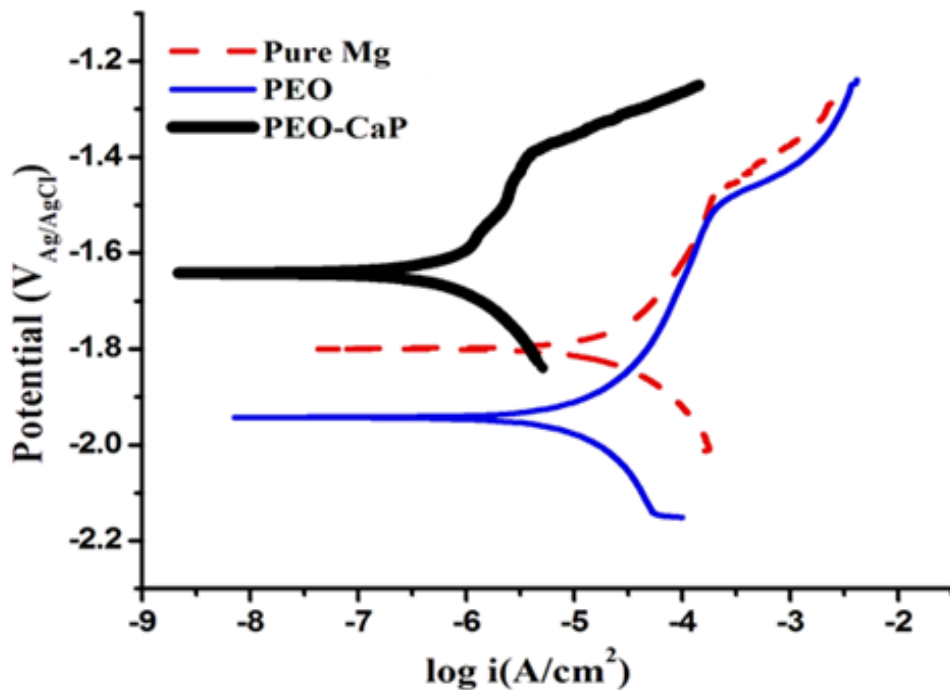


Figure 5.9 Potentiodynamic polarization plots of pure magnesium, PEO coated and PEO-CaP coated magnesium samples exposed to SBF.

Table 5.3 Electrochemical data for pure magnesium, PEO coated and PEO-CaP coated samples from potentiodynamic polarization curves.

Sample	E_{corr} (V _(Ag/AgCl))	i_{corr} ($\mu\text{A}/\text{cm}^2$)
Pure Mg	-1.8 \pm 0.02	23.5 \pm 3.6
PEO	-1.92 \pm 0.02	8.3 \pm 3
CaP-PEO	-1.66	0.85 \pm 0.07

Note: All experiments were conducted in triplicate and the standard deviations are provided with +/-.

5.2.5 EIS Long-term Degradation

In order to understand the longevity of the coating, long-term EIS experiments were conducted. The SBF was changed every 24 h during the test period to maintain the pH at 7.4. The R_p values for the samples at different time intervals are shown in Figure 5.10. For the pure magnesium, the R_p increased marginally from 510 $\Omega \text{ cm}^2$ (2 h) to 825 $\Omega \text{ cm}^2$ (24h), which can be attributed to the partial passivation during this exposure period. However, the R_p remained relatively stable with the increase in exposure period (1180 $\Omega \text{ cm}^2$ – 48 h).

Interestingly, the R_p of the PEO coated metal dropped significantly after 24 h exposure: 4300 $\Omega \cdot \text{cm}^2$ (2 h) to 780 $\Omega \cdot \text{cm}^2$ (24 h). It was noted that the R_p of the PEO coated metal after 24 h exposure is similar to that of the pure magnesium. The results revealed the poor long-term protective nature of the PEO coating. This suggests that chloride ions had slowly permeated through the porous layer and attacked the underneath compact MgO layer, as the R_p of the PEO coated metal was very low after 24 h exposure. On the other hand, the PEO-CaP coated metal showed significantly higher R_p as compared to the PEO coated metal, after 24 h exposure. The R_p of the PEO-CaP coated metal was $2 \times 10^4 \Omega \text{ cm}^2$: 97% higher than that of the PEO coated metal for same exposure time.

Although the R_p of the PEO-CaP coated metal decreased with increase in exposure period, the R_p recorded was more than one order of magnitude higher than the initial R_p of pure magnesium and two times higher than PEO coated metal, even after 72 h exposure to SBF.

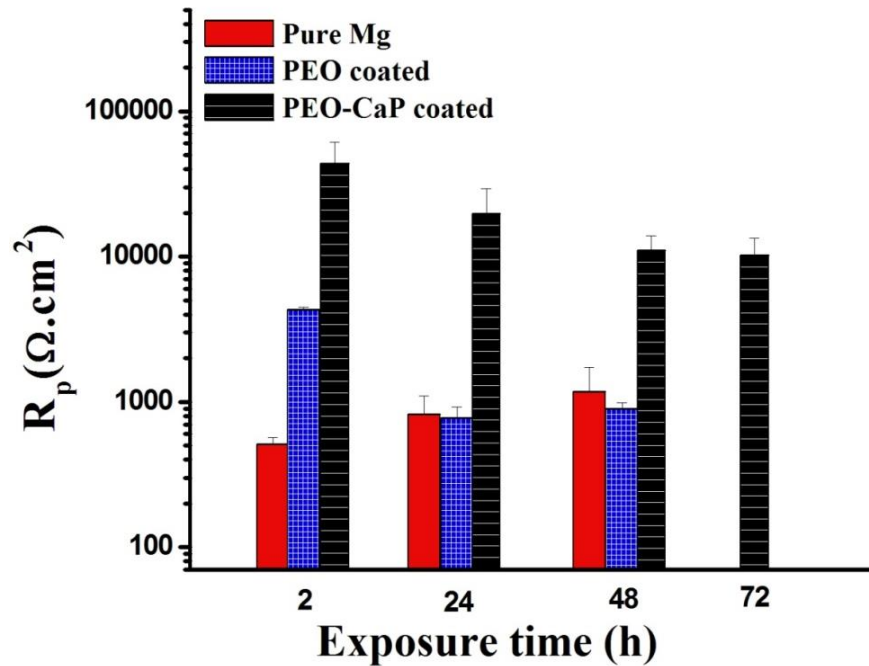


Figure 5.10 Polarization resistance (R_p) of pure magnesium, PEO coated and PEO-CaP coated magnesium samples after different immersion intervals in SBF.

5.2.6 Post-degradation Analysis

Figure 5.11 shows the post-degradation SEM micrographs of the PEO and the PEO-CaP coated samples. The PEO-coated metal did not show any major degradation attack on the surface. Only a few localized attacks were noticed, which suggest that the degradation was mainly underneath the PEO coating. It can be expected that the PEO layer would exfoliate when exposed for a longer period of time. However, the PEO-CaP coated metal did not show any sign of localized degradation. The porous nature of the underneath PEO coating was also not evident after 72 h exposure, which confirms

the protective nature of the CaP layer on the PEO layer. Hence, the dual layer inorganic coating (PEO-CaP) could be a suitable method to delay the degradation of the material.

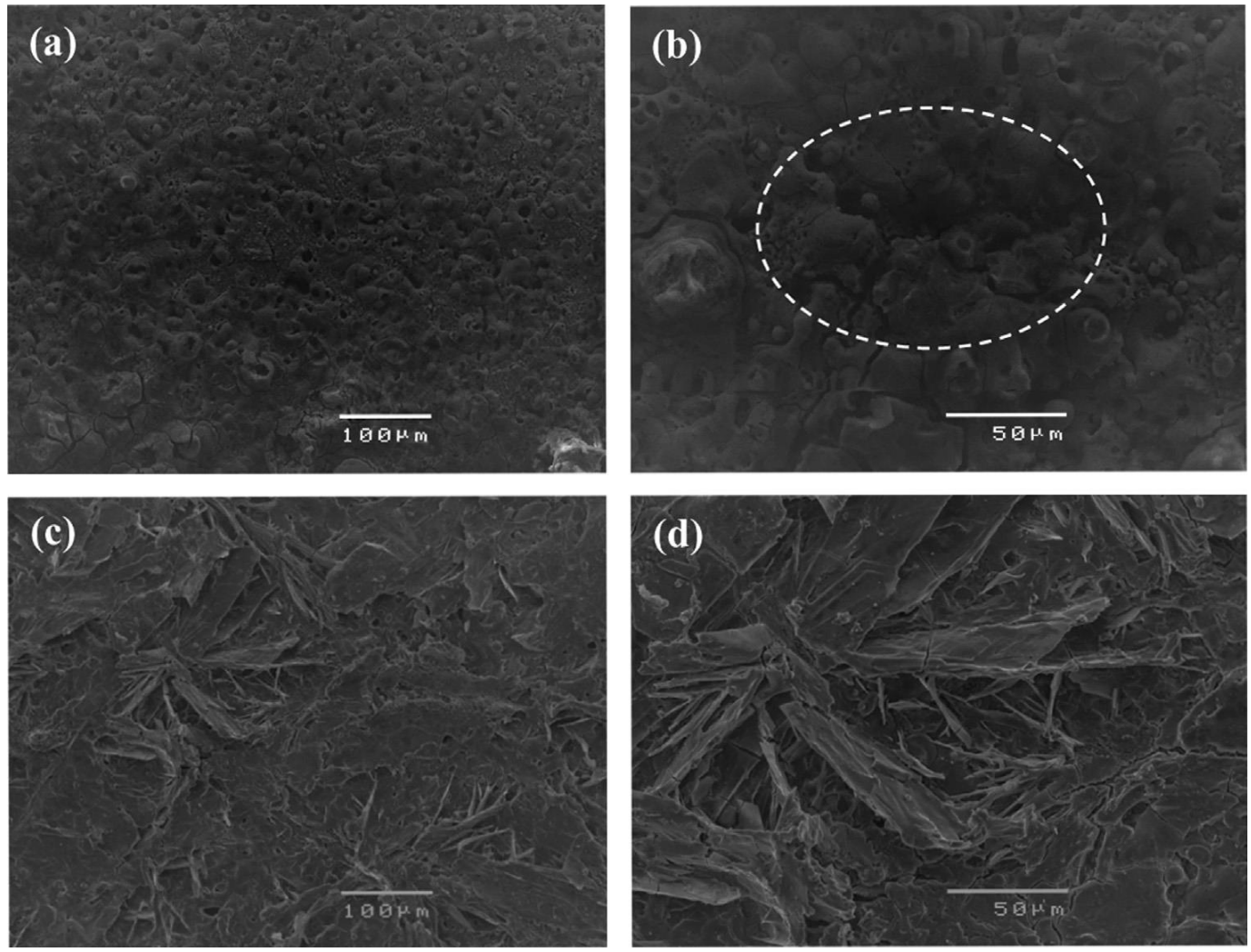


Figure 5.11 Post-degradation SEM micrographs of coated pure magnesium: (a and b) PEO coated, and (c and d) PEO-CaP coated.

5.3 Summary

Attempts were made to seal the porous silicate-based plasma electrolytic oxidation (PEO) layer on pure magnesium with biodegradable polymer and calcium phosphate to delay the localized degradation of magnesium in body fluid for better in-service mechanical integrity.

The PLLA coating on PEO coated magnesium has shown to be highly beneficial for improving the localized degradation resistance of the base material. While the corrosion current density (i_{corr}) of the pure magnesium was reduced by 65% with the PEO coating, the PEO-PLLA coating reduced the i_{corr} by almost 100%. As expected, the R_p of the PEO-PLLA Mg decreased with increase in exposure time. However, it was noted that the R_p of the PEO-PLLA Mg, even after 100 h, was 6 times higher than that of the PEO Mg after 48 h exposure, and did not show any visible localized attack.

The dual layer inorganic coating (PEO-CaP) was found to be very effective in delaying the general and localized degradation of the pure magnesium metal. The PEO-CaP coating improved the polarization resistance (R_p) by approximately two orders of magnitude and reduced the corrosion current density (i_{corr}) by ~96% as compared to that of the pure magnesium. Localized degradation was not evident on the PEO-CaP coated metal even after 72 h exposure to SBF.

CHAPTER 6 CONCLUSIONS

In order to enhance the performance of magnesium-based materials for biodegradable implant applications, polymer and ceramic materials were coated and tested under *in vitro* conditions. Polylactic acid (PLA) coated magnesium alloy, AZ91, applied using spin coating technique, has enhanced the degradation resistance of the alloy by more than one order of magnitude. Increasing the PLA coating thickness was found to increase the degradation resistance, but resulted in poor adhesion. Long-term EIS experiments of the PLA coated samples suggested that their degradation resistance gradually decreased with the increase in SBF exposure time, which can be attributed to the bulk degradation mechanism of PLA.

In the case of a silicate-based PEO coating on pure magnesium, the degradation resistance of the metal also increased by one order of magnitude. However, the performance of the PEO coating deteriorated drastically under long-term exposure. The porous outer layer allowed fluid penetration. Hence, an additional coating to seal the porous PEO layer was necessary. In this study, polymer and ceramic materials were used to seal the porous PEO layer. The electrochemical *in vitro* testing results showed that the dual layer coatings (PEO-PLA/ PEO-CaP) were very effective in not only reducing the general degradation even under long-term exposure, but also improved the localized degradation resistance, which is critical for load-bearing orthopedic implants.

REFERENCES

- Alabbasi, A., Kannan, M.B., Walter, R., Stormer, M., Blawert, C. (2013). "Performance of pulsed constant current silicate-based PEO coating on pure magnesium in simulated body fluid." *Mater. Lett.*, 106, 18-21.
- Alabbasi, A., Liyanaarachchi, S., Kannan, M.B. (2012). "Polylactic acid coating on a biodegradable magnesium alloy: An *in vitro* degradation study by electrochemical impedance spectroscopy." *Thin Solid Films*, 520, 6841-6844.
- Arrabal, R., Matykina, E., Hashimoto, T., Skeldon, P., Thompson, G.E. (2009). "Characterization of AC PEO coatings on magnesium alloys." *Surf. Coat. Tech.*, 203, 2207-2220.
- Beganskene, A., Sirutkaitis, V., Kurtinaitiene, M., Juskenas, R., Kareiva, A. (2004). "FTIR, TEM and NMR Investigations of Stöber silica nanoparticles." *Mater. Sci.*, 4, 287-290.
- Blawert, C., Sah, S.P., Liang, J., Huang, Y., Hoche, D. (2012). "Role of sintering and clay particle additions on coating formation during PEO processing of AM50 magnesium alloy." *Surf. Coat. Tech.*, 213, 48-58.
- Bonora, P. L., Deflorian, F., Fedrizzi, L. (1996). "Electrochemical Impedance Spectroscopy as a Tool for Investigating Underpaint Corrosion". *Electrochimica Acta*, 41, 1073-1082.
- Chandrasekar. M. S., Pushpavanam, M. (2008). "Pulse and pulse reverse plating- conceptual, advantages and applications." *Electrochim. Acta*, 53, 3313-3322.
- Chen, F., Zhou, H., Yao, B., Qin, Z., Zhang, Q. (2007). "Corrosion resistance property of the ceramic coating obtained through microarc oxidation on the AZ31 magnesium alloy surfaces." *Surf. Coat. Tech.*, 201, 4905-4908.
- Chen, Y., Song, Y., Zhang, S., Li, J., Zhao, C. (2011). "Interaction between a high purity magnesium surface and PCL and PLA coatings during dynamic degradation." *Biomed. Mater.*, 6,1.
- Chung, S.C., Cheng, J.R., Chiou, S.D., Shih, H.C. (2000). "EIS behaviour of anodized zinc in chloride environments." *Corros. Sci.*, 42, 1249-1468.
- Duan, H., Yan, C., Wang, F. (2007). "Effect of electrolyte additives on performance of plasma electrolytic oxidation films formed on magnesium alloy AZ91D." *Electrochim. Acta*, 52, 3785-3793.
- Duan, H., Yan, C., Wang, F. (2007). "Growth process of plasma electrolytic oxidation films formed on magnesium alloy AZ91D in silicate solution." *Electrochim. Acta*, 52, 5002-5009.

- Fontana, M.G. (1987). "Corrosion Engineering". 3rd Edition, McGraw-Hill International
- Ghasemi, A., Raja, V.S., Blawert, C., Dietzel, W., Kainer, K.U. (2008). "Study of the structure and corrosion behaviour of PEO coatings on AN50 magnesium alloy by electrochemical impedance spectroscopy." *Surf. Coat. Tech.*, 202, 3513-3518.
- Groot, K.D., Wolke, J.G.C., Jansen, J.A. (1998). "Calcium phosphate coatings for medical implants." *P. I. Mech. Eng.*, 212, 137-147.
- Guo, L.F., Yue, T.M., Man, H.C. (2005). "Excimer laser surface treatment of magnesium alloy WE43 for corrosion resistance improvement." *J. Mater. Sci.*, 40, 3531-3533.
- Gupta, B., Revagade, N., Hilborn, J. (2007). "Poly(lactic acid) fiber: An overview." *Prog. Polym. Sci.*, 32, 455-482.
- Gu, X.N., Li, N., Zhou, W.R., Zheng, Y.F., Zhao, X., Cai, Q.Z., Ruan, L. (2011). "Corrosion resistance and surface biocompatibility of a microarc oxidation coating on a Mg-Ca alloy." *Acta Biomater.*, 7, 1880-1889.
- Gu, Yanhong., Chen, C., Bandopadhyay, S., Ning, C., Zhang, Y., Guo, Y. (2012). "Corrosion mechanism and model of pulsed DC microarc oxidation treated AZ31 alloy in simulated body fluid." *Appl. Surf. Sci.*, 258, 6116-6126.
- Hong, J., Park, H. (2011). "Fabrication and characterization of block copolymer micelle multilayer films prepared using dip-, spin- and spray –assisted layer-by-layer assembly deposition." *Colloids Surf., A*, 381, 7-12.
- Hornberger, H., Virtanen, S., Boccaccini, A.R. (2012). "Biomedical coatings on magnesium alloys-A review." *Acta Biomater.*, 8, 2442-2455.
- Jin, S., Amira, S., Ghali, E. (2007). "Electrochemical impedance spectroscopy evolution of the corrosion behaviour of die cast and thixocast AXJ530 magnesium alloy." *Adv. Eng. Mater.*, 9, 75-83.
- Kannan, M. B. (2012a). "Improving the packing density of calcium phosphate coating on a magnesium alloy for enhanced degradation resistance." *J. Biomed. Mater. Res.-A*, 101A, 1248-1254.
- Kannan, M.B. (2012b). "Enhancing the performance of calcium phosphate coating on a magnesium alloy for bio implant applications." *Mater. Lett.*, 76, 109-112.
- Kannan, M. B. (2010). "Influence of microstructure on the in-vitro degradation behaviour of magnesium alloys." *Mater. Lett.*, 64, 739-742.
- Kannan, M.B., Dietzel, W. (2012). "Pitting-induced hydrogen embrittlement of magnesium-aluminium alloy." *Mater. Des.*, 42, 321-326.

- Kannan, M.B., Liyanaarachchi, S. (2013). "Hybrid coating on a magnesium alloy for minimizing the localized degradation for load-bearing bridgeable mini-implant applications". *Materials Chemistry and Physics* 142 (1), 350-354.
- Kannan, M. B., Orr, L. (2011). "*In vitro* mechanical integrity of hydroxyapatite coated magnesium alloy." *Biomed. Mater.*, 6, 11, 045003.
- Kannan, M. B., Raman R.K.S. (2008a). "*In vitro* degradation and mechanical integrity of calcium-containing magnesium alloys in modified-simulated body fluid." *Biomaterials*, 29, 2306-2314.
- Kannan, M. B., Raman R.K.S. (2008b). "Evaluation of stress corrosion cracking behaviour of AZ91 alloy in modified –simulated body fluid for orthopaedic implant application." *Scripta Mater.*, 59, 175-178.
- Kannan, M. B., Wallipa, O. (2012). "Potentiostatic pulse-deposition of calcium phosphate on magnesium alloy for temporary implant applications-An *in vitro* corrosion study." *Mat. Sci. Eng. C-Biomim.*, 33, 675-679.
- Kirkland, N.T., Lespagnol, J., Birbilis, N., Staiger, M.P. (2010). "A survey of bio-corrosion rates of magnesium alloys." *Corros. Sci.*, 52, 287-291.
- Kuo, M.C, Yen.S.K. (2002). "The process of electrochemical deposited hydroxyapatite coatings on biomedical titanium at room temperature." *Mat. Sci. Eng. C-Biomim.*, 20, 153-160.
- Liang, J., Srinivasan, P.B., Blawert, C., Stormer, M., Dietzel, W. (2009). "Electrochemical corrosion behaviour of plasma electrolytic oxidation coatings on AM50 magnesium alloy formed in silicate and phosphate based electrolytes." *Electrochim.Acta*, 54, 3842-3850.
- Liang, J., Srinivasan, P.B., Blawert, C., Dietzel, W. (2010). "Influence of chloride ion concentration on the electrochemical corrosion behaviour of plasma electrolytic oxidation coated AM50 magnesium alloy." *Electrochim. Acta*, 55, 6802-6811.
- Liu, D. M., Yang, Q., Troczynski, T., (2002). "Sol-gel hydroxyapatite coating on stainless steel substrates." *Biomaterials*, 20, 691-698.
- Liu, G.Y., Hu, J., Ding, Z.K., Wang, C. (2011). "Bioactive calcium phosphate coating formed on micro-arc oxidized magnesium by chemical deposition." *Appl. Surf. Sci.*, 257, 2051-2057.
- Lunt, J. (1998). "Large-scale production, properties and commercial applications of polylactic acid polymers." *Polym. Degrad. Stabil.*, 59, 145-152.
- Lu, P., Cao, L., Xu, X., Wu, X. (2011). "Evaluation of magnesium ions release, biocorrosion, and hemocompatibility of MAO/PLLA-modified magnesium alloy WE42." *Biomed.Mater. Res.*, 96B, 101-109.

- Magalhaes, A.A.O., Margarit, I.C.P., Mattos, O.R. (1999). "Electrochemical characterization of chromate coatings galvanized steel." *Electrochim. Acta*, 44, 4281-4287.
- Middleton, J.C., Tipton, A.J. (2000). "Synthetic biodegradable polymers as orthopaedic devices." *Biomaterials*, 21, 2335-2346.
- Nair, L.S., Laurencin, C.T. (2007). "Biodegradable polymers as biomaterials." *Prog. Polym. Sci.*, 32, 762-798.
- Orazem, M.E. Tribollet, B. (2008). "Electrochemical Impedance Spectroscopy", A John Wiley & Sons, Inc. Publication.
- Redepenning, J., Schlessinger, T., Burnham, S., Lippiello, L., Miyano, J. (1996). "Characterization of electrolytically prepared brushite and hydroxyapatite coatings on orthopaedic alloys". *J. Biomed. Mater. Res.*, 30, 287-294.
- Saris, N.E.L., Mervaala, E., Karppanen, H., Khawaja, J.A., Lewenstam, A. (2000). "Magnesium: an update on physiological, clinical and analytical aspects." *Clin. Chim. Acta*, 294, 1-26.
- Shi, D. (2004). "Biomaterials and Tissue Engineering." Berlin: Springer.
- Song, G. (2007). "Control of biodegradation of biocompatible magnesium alloys." *Corros. Sci.*, 49, 1696-1701.
- Song, G., Atrens, A. (2003). "Understanding magnesium corrosion." *Adv. Eng. Mater.*, 5, 837-858.
- Srinivasan, P.B., Liang, J., Blawert, C., Stormer, M., Dietzel, W. (2009). "Effect of current density on the microstructure and corrosion behaviour of plasma electrolytic oxidation treated AM50 magnesium alloy." *Appl. Surf. Sci.*, 255, 4212-4218.
- Staiger, M.P., Pietak, A.M., Huadmai, J., Dias, G. (2006). "Magnesium and its alloys as orthopaedic biomaterials: a review." *Biomaterials*, 27, 1728-1734.
- Walter, R., Kannan, M.B. (2011). "In-vitro degradation behaviour of WE54 magnesium alloy in simulated body fluid." *Mater. Lett.*, 65, 748-750.
- Wang, H., Guan, S., Wang, X., Ren, C., Wang, L. (2010). "*In vitro* degradation behaviour of Ca-deficient hydroxyapatite coated Mg-Zn-Ca alloy for bone implant application." *Acta Biomater.*, 6, 1743-1748.
- Wang, Y.M., Wang, F.H., Xu, M.J., Zhao, B., Guo, L.X., Ouyang, J.H. (2009). "Microstructure and corrosion behaviour of coated AZ91 alloy by microarc oxidation for biomedical application." *Appl. Surf. Sci.*, 255, 9124-9131.

Witte, F., Hort, N., Vogt, C., Cohen, S., Kainer, K.U., Willumeit, R., Feyerabend, F. (2008). "Degradable biomaterials based on magnesium corrosion." *Curr.Opin.Solid. St. M.*, 12, 63-72.

Witte, F., Kaese, V., Haferkamp, H., Switzer, E., Meyer-Lindenberg, A., Wirth, C.J., Windhagen, H. (2005). "In vivo corrosion of four magnesium alloys and the associated bone response." *Biomaterials*, 26, 3557-3563.

Wolf, F., Cittadini, A. (2003). "Chemistry and biochemistry of magnesium." *Mol. Aspects Med.*, 24, 3-9.

Yerokhin, A.L., Nie, X., Leyland, A., Matthews, A., Dowey, S. J. (1999). "Plasma electrolysis for surface engineering." *Surf.Coat. Tech.*, 122, 73-93.

Ying-ying, H., Min, Q., Meng, Z., Hong-ze, L., Da-zhi, Y. (2006). "Degradation mechanisms of poly (lactic-co-glycolic acid) films *in vitro* under static and dynamic environment." *Trans. Nonferrous Met. Soc. China*, 16, s293-s297.

Zeng, L., Yang, S., Zhang, W., Guo, Y., Yan, C. (2010). "Preparation and characterization of a double-layer coating on magnesium alloy AZ91D." *Electrochim.Acta*, 55, 3376-3383.

Zeng, R., Dietzel, W., Witte, F., Hort, N. (2008). "Progress and challenge for magnesium alloys as biomaterials." *Adv. Eng. Mater.*, 10, B13-14.

Zhang, X., Wyss, U.P., Pichora, D., Goosen, M.F.A. (1994). "An investigation of poly(lactic acid) degradation." *J. Bioact. Compat. Pol.*, 9, 80-100.

Zucchi, F., Grassi, V., Frignani, A., Monticelli, C., Trabanelli, G. (2006). "Electrochemical behaviour of a magnesium alloy containing rare earth elements." *J.Appl. Electrochem.*, 36, 195-204.